An aspartyl cathepsin, *CTH3*, is essential for proprotein processing during secretory granule maturation in *Tetrahymena thermophila*

Santosh Kumar, Joseph S. Briguglio, and Aaron P. Turkewitz
Department of Molecular Genetics and Cell Biology, University of Chicago, Chicago, IL 60637

ABSTRACT **In *Tetrahymena thermophila*, peptides secreted via dense-core granules, called mucocysts, are generated by proprotein processing. We used expression profiling to identify candidate processing enzymes, which localized as cyan fluorescent protein fusions to mucocysts. Of note, the aspartyl cathepsin Cth3p plays a key role in mucocyst-based secretion, since knockdown of this gene blocked proteolytic maturation of the entire set of mucocyst proproteins and dramatically reduced mucocyst accumulation. The activity of Cth3p was eliminated by mutation of two predicted active-site mutations, and overexpression of the wild-type gene, but not the catalytic-site mutant, partially rescued a Mendelian mutant defective in mucocyst proprotein processing. Our results provide the first direct evidence for the role of proprotein processing in this system. Of interest, both localization and the *CTH3* disruption phenotype suggest that the enzyme provides non–mucocyst-related functions. Phylogenetic analysis of the *T. thermophila* cathepsins, combined with prior work on the role of sortilin receptors in mucocyst biogenesis, suggests that repurposing of lysosomal enzymes was an important step in the evolution of secretory granules in ciliates.**

Monitoring Editor
Adam Linstedt
Carnegie Mellon University

Received: Mar 27, 2014
Revised: Jun 11, 2014
Accepted: Jun 13, 2014

INTRODUCTION

In humans and other animals, a large and diverse set of secreted peptides, including hormones and neuropeptides, play key roles in intercellular communication and tissue coordination. The peptides are generated, stored, and released upon demand from secretory organelles called secretory granules. Thus the mechanisms underlying granule formation are of key physiological significance (Arvan and Castle, 1998; Kim *et al.*, 2006; Bonnemaison *et al.*, 2013). In addition, elucidating these mechanisms may also shed light on the evolution of cell type–specific features in the eukaryotic secretory pathway, since secretory granules represent an example of the contribution of adaptations in protein traffic to establishing distinct cellular niches.

The formation of secretory granules depends on a multistep pathway (Molinete *et al.*, 2000; Tooze *et al.*, 2001; Morvan and Tooze, 2008). First, newly synthesized polypeptides, such as proinsulin, are sorted as aggregates, at the level of the *trans*-Golgi network or during subsequent maturation, into vesicles that are distinct from those bearing soluble cargo destined for rapid constitutive secretion or for lysosomes (Orci *et al.*, 1987; Chanat and Huttner, 1991; Arvan and Castle, 1998). A maturation process remodels the aggregates into a highly condensed assembly, creating the eponymous dense core within the vesicle lumen (Orci *et al.*, 1985; Michael *et al.*, 1987; Bendayan, 1989; Dodson and Steiner, 1998). At a biochemical level, maturation is an interval during which the bioactive peptides are generated from proproteins by proteolytic processing. The best-studied enzymes are the endoproteases called pro–hormone convertases, which are targeted to and activated in immature secretory vesicles (Steiner, 1998; Crump *et al.*, 2001). The prohormone convertases are related to a ubiquitous aspartyl protease in the animal secretory pathway—furin—and are more distantly related to bacterial subtilisins (Steiner, 1991; Creemers *et al.*, 1998). In addition, proprotein processing in neuropeptide-containing secretory granules involves the cysteine protease cathepsin L (Hook *et al.*, 2008). At the cell biological level, maturation also includes the withdrawal, via vesicle budding, of both missorted soluble constituents

This article was published online ahead of print in MBoC in Press (http://www.molbiolcell.org/cgi/doi/10.1091/mbc.E14-03-0833) on June 18, 2014.

Address correspondence to: Aaron P. Turkewitz (apturkew@midway.uchicago.edu).

Abbreviations used: CFP, cyan fluorescent protein; GFP, green fluorescent protein; GRL, granule lattice; GRT, granule tip; RT-PCR, reverse transcription PCR.

and secretory granule maturation factors, such as the convertases, which can thus be recycled (Klumperman *et al.*, 1998; Molinete *et al.*, 2000; Ahras *et al.*, 2006). The mature granule must also possess a variety of membrane proteins, including those that specify docking and subsequent stimulus-dependent fusion at the plasma membrane.

Secretory granules are found in just a subset of animal tissues, especially in neuroendocrine tissues, but similar organelles have been noted in a variety of eukaryotic lineages, although few of these have been analyzed at the molecular level (Elde *et al.*, 2007). The most extensive studies have been in the ciliates *Tetrahymena thermophila* and *Paramecium tetraurelia*, in which secretory organelles with dense cores, called mucocysts and trichocysts, respectively, undergo stimulated exocytosis during predator–prey encounters but may also serve other functions (Adoutte, 1988; Knoll *et al.*, 1991; Vayssie *et al.*, 2000; Turkewitz, 2004). Of note, the process of mucocyst/trichocyst formation shares striking similarities to insulin granule formation in mammalian pancreatic β cells, including an apparent role for proteolytic maturation of proproteins during core formation (Collins and Wilhelm, 1981; Adoutte *et al.*, 1984). Comparison of ciliate proproteins versus the processed products identified conserved motifs that are likely to be targets of multiple proteases (Madeddu *et al.*, 1994; Gautier *et al.*, 1996; Verbsky and Turkewitz, 1998), an inference also consistent with results using class-specific protease inhibitors (Bradshaw *et al.*, 2003), and led to a model for stepwise assembly of the granule core in *Paramecium* (Vayssie *et al.*, 2001). Unfortunately, in all these studies the ciliate processing enzymes themselves could only be inferred. They are unlikely to be related to mammalian prohormone convertases, for which no homologue has been identified in a ciliate genome.

In *T. thermophila*, the mucocyst cargo proteins are encoded by two multigene families, called *GRL* (for granule lattice) and *GRT* (for granule tip; Bowman *et al.*, 2005b; Cowan *et al.*, 2005). The Grl proteins constitute the dense core and are the substrates for proteolytic processing during mucocyst maturation. The *GRL* and *GRT* genes are coordinately transcribed under a range of conditions (Rahaman *et al.*, 2009). Moreover, a screen for additional coregulated genes uncovered a receptor in the sortilin/VPS10 family that is required for Grt sorting to mucocysts (Briguglio *et al.*, 2013).

In the work described in this article, we used expression profiling to identify candidates for mucocyst processing enzymes. We focus on one of the aspartyl cathepsins, *CTH3*, which plays a key role in the processing of pro-Grl proteins and is essential for both mucocyst biogenesis and exocytosis.

RESULTS

Expression profiling reveals candidates for proprotein processing enzymes in *T. thermophila*

The >24,000 genes predicted in the *T. thermophila* macronuclear genome include a large number of putative proteases, including 43 aspartic proteases belonging to two subfamilies, 211 cysteine proteases belonging to 11 subfamilies, 139 metalloproteases belonging to 14 subfamilies, 73 serine proteases belonging to 12 subfamilies, and 14 threonine proteases (Eisen *et al.*, 2006; Coyne *et al.*, 2008; unpublished data). Many of these have predicted signal sequences and are therefore likely to be secreted and/or function within digestive organelles, but a subset may be specialized for mucocyst biogenesis. Genes encoding several classes of mucocyst components are coregulated (Haddad *et al.*, 2002; Rahaman *et al.*, 2009). We therefore used the online tools at the *Tetrahymena* Gene Expression Database (TGED; http://tged.ihb.ac.cn/), subsequently reorganized at the *Tetrahymena* Functional Genomics Database (TetraFGD; http://tfgd.ihb.ac.cn/), to ask whether any putative proteases are also coregulated with *GRL* genes. We identified four cathepsins (*CTH1–4*) and one carboxypeptidase (*CAR1*) whose expression profiles are striking similar to those of *GRL* genes (Figure 1A) but distinct from those of other, closely related proteases (Figure 1B).

All of the enzymes possess likely N-terminal signal sequences consistent with translocation into the secretory pathway (Figure 1C). Three of the four cathepsins (*CTH1–3*) belong to the aspartyl-protease subgroup, whereas *CTH4* belongs to the cysteine-protease subgroup (cathepsin C family). Another cysteine protease, cathepsin B, was previously studied in *Tetrahymena* and shown to localize to food vacuoles (Jacobs *et al.*, 2006). We added this gene to our analysis as an example of a nonmucocyst protease.

The aspartyl cathepsins, on which we focused our attention, have conserved catalytic motifs that are characteristic of this subfamily, including two catalytic aspartic acid residues in the conserved motifs DTG/DTG and DTG/DSG (Figure 1C). The identification of the conserved motifs was also supported by primary sequence alignment between the *Tetrahymena* aspartyl proteases and *Homo sapiens* aspartic proteases (Supplemental Figure S1). The cysteine proteases possess conserved triad catalytic residues (C, H, N; Figure 1C). The Car1p sequence contains a putative catalytic glutamate (E) at an appropriate position, but this is weakly determined, given the minimal size of this motif and the limited overall sequence identity with characterized carboxypeptidases in other nonciliate species.

The phylogenetic relationships between the *Tetrahymena* aspartyl proteases and a set of related enzymes from other eukaryotes are shown in Figure 2. The aspartyl cathepsins *CTH1–3* fall within a cluster of genes from ciliates and the related apicomplexan parasites (Figure 2). The carboxypeptidase *CAR1* has close homologues only in other ciliates (*Ichthyophthirius multifiliis* and *P. tetraurelia*; Supplemental Figure S2). Phylogenetic analysis therefore suggests that the aspartyl cathepsin family underwent a large expansion within the alveolates (ciliates, apicomplexans, and dinoflagellates), whereas the carboxypeptidase family expanded in ciliates after they had branched from apicomplexans.

Gene disruption implicates each of the aspartyl cathepsins in mucocyst biogenesis, with a special role for *CTH3*

We targeted each of the candidate protease genes for disruption via homologous recombination with a drug-resistance cassette (Figure 3A). This standard approach results in gradual replacement with the disrupted allele over roughly 3–4 wk of growth in drug of all ~45 expressed copies in the polyploid macronucleus, producing a functional knockout (Cassidy-Hanley *et al.*, 1997). The process of allele replacement depends on the random assortment of alleles to the two daughters at each cell division, a feature of *Tetrahymena* macronuclei (Karrer, 2000). If a gene is essential for cell viability, one cannot recover daughters in which all intact macronuclear copies have been replaced.

To assess the extent of gene expression, we used reverse transcription PCR (RT-PCR) to monitor the knockout strains. For *CAR1*, no RT-PCR product could be detected in the putative knockouts, indicating that the disruption was complete (Figure 3B). *CAR1*-knockout cells (Δ*car1*) showed a modest growth phenotype (Supplemental Table S1). The cathepsin-knockout lines all showed low levels of RT-PCR product of the targeted genes, even after extended growth in drug. In all cases, the apparent reduction in the relevant gene transcript was >90% relative to wild type (*CTH1*, 92%; *CTH2*, 96%; *CTH3*, 95%; Figure 3B). The persistent low-level RT-PCR products may reflect the inability to replace all macronuclear alleles or

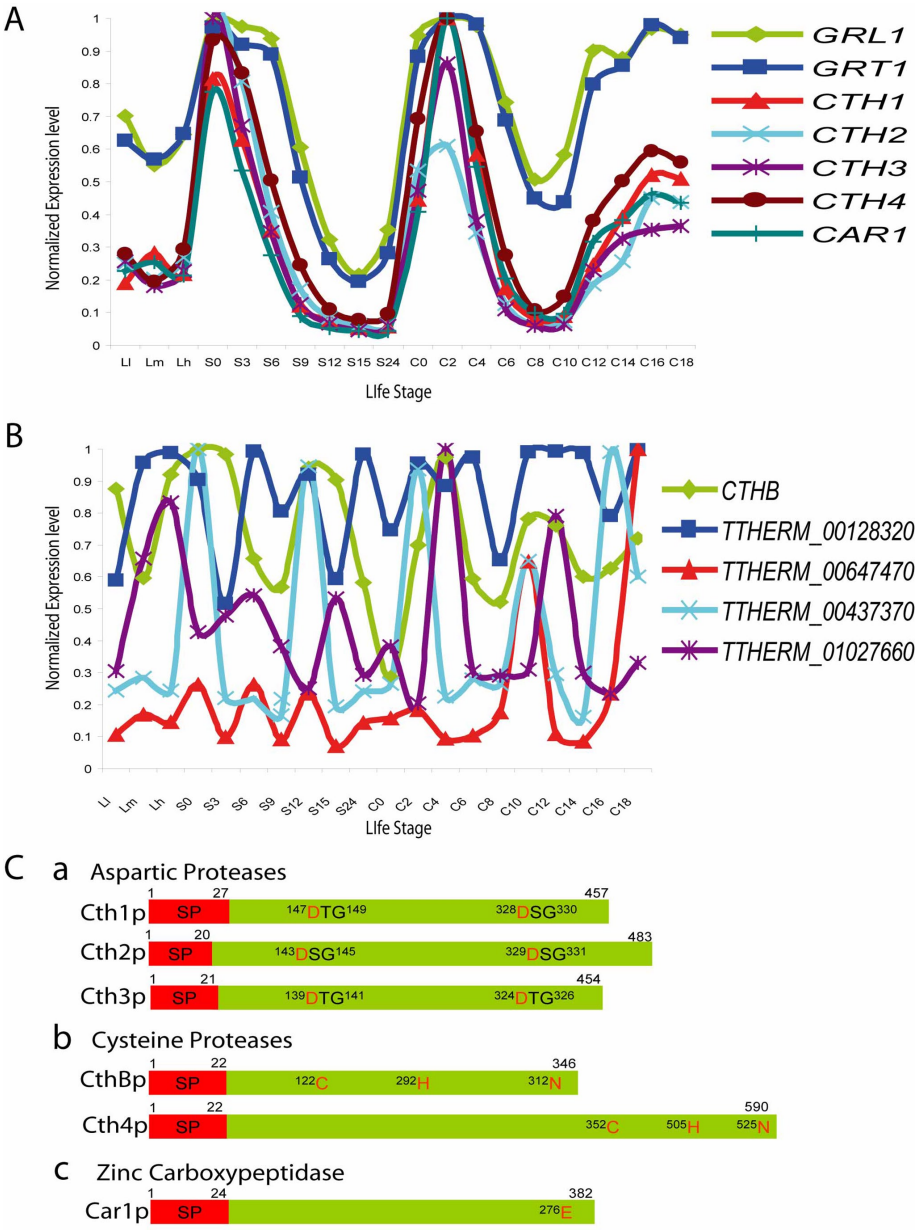

FIGURE 1: Expression profiling identifies a set of enzymes that are coregulated with secretory granule cargo genes. (A) The expression profiles of four predicted cathepsin genes (*CTH1–4*) and one carboxypeptidase (*CAR1*) are very similar to those of *GRL1* and *GRT1*, genes that encode mucocyst cargo proteins. The profiles of transcript abundance under a variety of culture conditions, derived via hybridization of stage-specific cDNAs to whole-genome microarrays, were downloaded from the *Tetrahymena* Functional Genomics Database. In the plots here, each trace was normalized to that gene's maximum expression level. The culture conditions sampled at successive time points represent growing (L-l, L-m, and L-h), starved (S-0, S-3, S-6, S-9, S-12, S-15, and S-24), and conjugating (C-0, C-2, C-4, C-6, C-8, C-10, C-12, C-14, C-16, and C-18) cultures. Details on the sampling times are found in Miao *et al.*, 2009. (B) The remainder of the predicted protease-encoding genes are not coregulated with mucocyst-related genes. For example, the expression profiles of four aspartic proteases (TTHERM_00128320, 00647470, 00437370, 01027660) and a cysteine protease (*CTHB*) are distinct from those in A. (C) In silico–predicted features of Cth1p, Cth2p, Cth3p, Cth4p, CthB, and Car1p. Features include N-terminal endoplasmic reticulum translocation signal peptides, the catalytic triplet (DTG or DSG) of aspartic proteases, catalytic residues (C, H, N) of cysteine proteases, and the catalytic residue (E) of zinc carboxypeptidases. The signal peptides shown for Cth1p and CthB are not robustly predicted by SignalP (values of 0.48 and 0.35, respectively, compared with the threshold value for signal peptides of 0.5). Nonetheless, the N-terminal sequences of Cth1p shown in Supplemental Figure S1 appear to have the expected features of a signal peptide.

may be artifacts arising from inefficient amplification of intact related members within these large gene families or from amplification of the intact (but silent) copies of the genes that persist in the micronucleus. We concluded that a minimum of >90% knockdown was sufficient to analyze the potential roles of these candidate genes. Only the cells targeted for *CTH3* knockout showed an increase in doubling time, confirmed for multiple clones (Supplemental Table S1), indicating that *CTH3* may be important for growth under these culture conditions.

To ask whether any of these genes is involved in mucocyst secretion, we first tested the exocytic response using a semiquantitative assay based on stimulation by dibucaine, which triggers mucocyst exocytosis (Satir, 1977; Cowan *et al.*, 2005). When wild-type cells are exposed briefly to dibucaine, the mucocyst contents are released as macroscopic protein aggregates and can be visualized after low-speed centrifugation as a thick, flocculent layer (Figure 4, A and B). Parallel treatment of the mutant lines showed that the Δ*car1* mutant was identical to wild type (Figure 4B, iv, right). The *cth1* and *2*–knockout strains showed flocculent release that was reduced compared with wild type (Figure 4B, i and ii, right). Most dramatically, flocculent release was completely absent from the Δ*cth3* mutant strain (Figure 4B, iii, right). For that reason we focused further studies on the *CTH3* gene, using the *CAR1* and cathepsin B (*CTHB*) genes as controls in some experiments.

Localization of cyan fluorescent protein–tagged processing protease candidates reveals mucocyst localization

Tetrahymena mucocysts are elongated (1 × 0.2 μm) vesicles that dock at regularly arrayed sites at the cell periphery (Allen, 1967). We determined the localization of Cth3p, in addition to that of Car1p and CthB, by expressing each as a cyan fluorescent protein (CFP) fusion controlled by a cadmium-inducible metallothionein (*MTT1*) promoter (Shang *et al.*, 2002). Overnight induction of the Cth3p and Car1p constructs resulted in CFP localization to docked mucocysts (Figure 5A, top and middle). The same results were obtained with Cth1p, Cth2p, and Cth4p (unpublished data). In contrast, cathepsin B, when expressed in the identical construct, showed little or no cortical localization but instead was found in cytoplasmic structures, including food vacuoles, consistent with prior characterization (Jacobs *et al.*, 2006; Figure 5A, bottom).

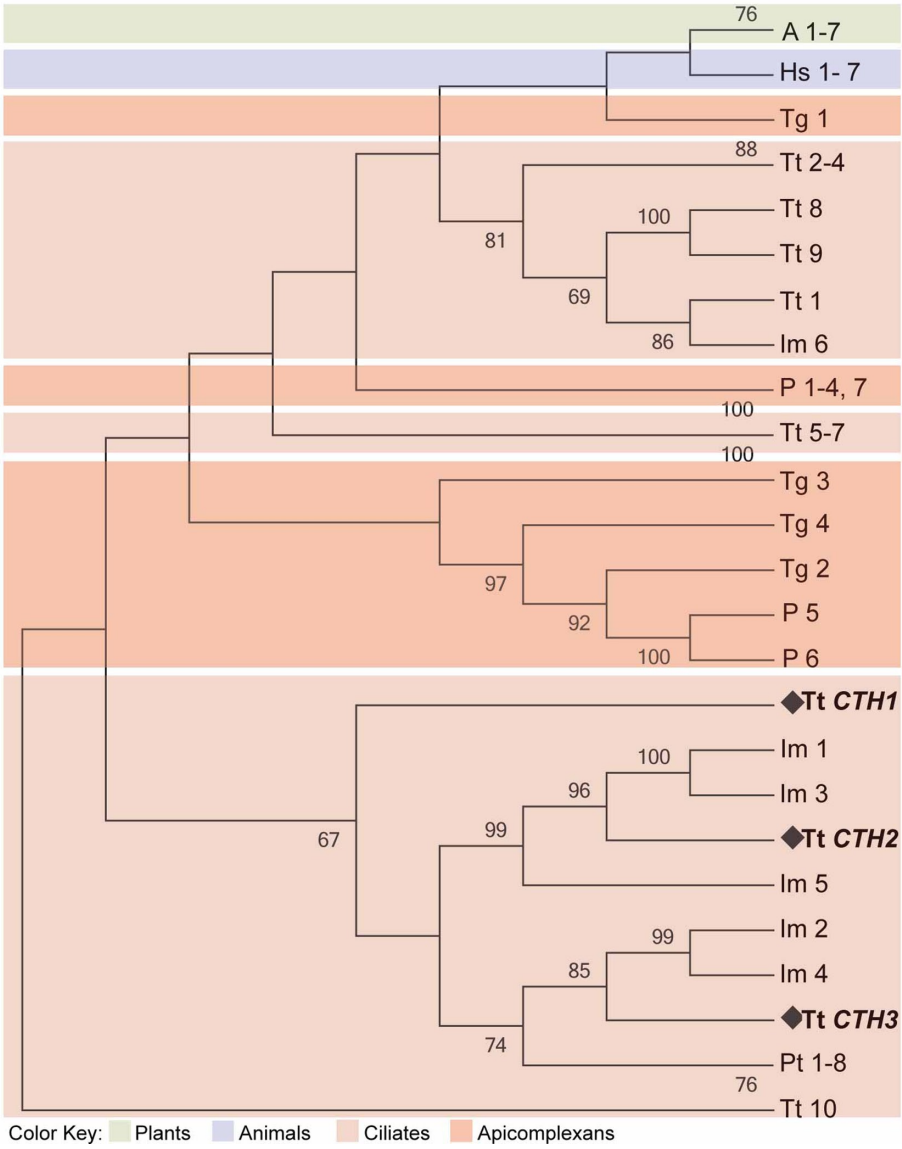

FIGURE 2: Phylogenetic reconstruction of aspartyl cathepsin genes. The maximum-likelihood tree illustrates the phylogenetic relationship between aspartyl cathepsins in ciliates, apicomplexans, *Arabidopsis* species, and *H. sapiens*. The *T. thermophila* aspartyl cathepsins *CTH1*, *CTH2*, and *CTH3* are in boldface. Blocks of cathepsins that fall within single lineages or a group of closely related lineages are shown in color blocks (see color key at bottom of figure). *T. gondii* (Tg), *Plasmodium* spp. (P), *Arabidopsis* spp. (A), *H. sapiens* (Hs), *T. thermophila* (Tt), *P. tetraurelia* (Pt), *I. multifiliis* (Im). See Supplemental Table S3 for a list of accession numbers for all sequences.

Of interest, Western blotting of cell lysates from clones visualized in Figure 5A, in which fusion protein expression had been induced overnight, revealed that the fusion proteins had themselves undergone likely proteolytic processing. That is, CFP immunoreactivity was detected predominantly in bands of the size expected for a CFP monomer rather than the sizes expected for the engineered fusion proteins (Figure 5B). In the case of the cathepsin B fusion, the low level of monomeric CFP is consistent with the fusion protein being delivered to the food vacuole, a degradative compartment. To confirm that monomeric CFP in each line was derived from a full-length fusion protein, we repeated the Western blotting analysis but with cells in which transgene expression was induced for just 2 h. Under those conditions, most CFP immunoreactivity was present in bands of the sizes expected for the full fusion proteins (Figure 5C). At that time point, Cth3p and Car1p showed extensive colocalization with the mucocyst core protein Grl3p. In contrast, Grl3p showed little colocalization with CthB-CFP (Figure 5D). Supplemental Movies S1–S3 show consecutive optical sections of these samples. These results indicate that Cth3p and Car1p, but not CthBp, localize to mucocysts or intermediates in mucocyst maturation.

Cathepsin 3 is required for mucocyst formation

In fixed permeabilized cells, mucocysts can be labeled with two monoclonal antibodies (mAbs) that recognize, respectively, members of the two major families of mucocyst cargo proteins. Grl3p, recognized by mAb 5E9, belongs to the Grl family of proteins that undergo proteolytic processing (Cowan *et al.*, 2005). Grt1p, recognized by mAb 4D11, belongs to the Grt family of mucocyst proteins (Bowman *et al.*, 2005a,b). Grt1p does not undergo processing, and in mature mucocysts it localizes to the tip that docks with the plasma membrane (Bowman *et al.*, 2005a). Staining of wild-type cells with either the anti-Grt1p or anti-Grl3p mAb reveals the array of mucocysts, with nearly the entire set docked at the cell periphery as seen in cell cross section (Figure 6, top). The same pattern was seen in Δ*car1* cells, consistent with the normal exocytic response in these cells (Figure 6, bottom). In contrast, the *cth3* mutant showed dramatically reduced accumulation of both mucocyst cargo proteins (Figure 6, middle). Of note, much of the Grl3p in the Δ*cth3* mutant is present in intracellular puncta. These may represent aberrant or arrested intermediates in mucocyst biosynthesis. However, they do not contain visible Grt1p, since the low level of that protein is restricted to puncta near the plasma membrane. Similarly, a small number of cortical puncta were seen with immunostaining for Grl3p. The elongated profiles of the cortical puncta suggest they may correspond to mucocysts, and electron microscopy of thin sections from Δ*cth3* cells indeed showed occasional docked mucocysts indistinguishable from wild type (unpublished data).

To ask whether the Grl3p-positive vesicles present in Δ*cth3* cells undergo exocytosis upon stimulation, we treated the cells with the polycationic dye Alcian blue. When wild-type cells are exposed to Alcian blue, they become entrapped in robust capsules formed by the dye-dependent cross-linking of the exocytosed mucocyst contents (Tiedtke, 1976). Because of the high affinity of Alcian blue for mucocyst contents, this reagent can be used to detect mucocyst exocytosis even in mutants that show greatly reduced stimulated mucocyst discharge (Melia *et al.*, 1998). When we treated wild-type, Δ*car1*, and Δ*cth3* cells with Alcian blue, virtually 100% of cells from

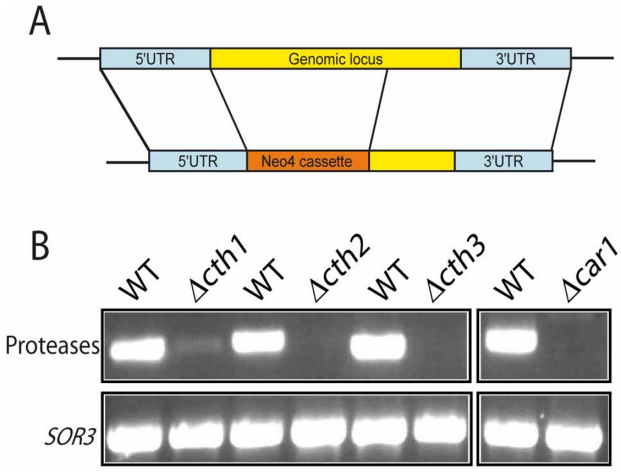

FIGURE 3: Disruption of *CTH1-3* and *CAR1*. (A) Schematic of gene-knockout constructs. Replacements of the *CTH1-3* and *CAR1* genes by the Neo4 drug resistance cassette were targeted by homologous recombination. A detailed description of the construction and use of the *CTH1–3* and *CAR1* knockout constructs is in *Materials and Methods*. (B) Verification of gene knockouts by RT-PCR. RNA was extracted from wild type, Δ*cth1*, Δ*cth2*, Δ*cth3*, and Δ*car1*, subjected to coupled reverse transcription, and PCR amplified using primers listed in Supplemental Table S2. As shown in this 1% ethidium bromide–stained agarose gel, each of the gene-knockout lines showed either complete or near-complete absence of the product corresponding to the targeted gene. To confirm amplification of equal amounts of cDNA, RT-PCR with primers specific for *SOR3* were run in parallel.

wild-type and Δ*car1* cultures were surrounded by visible blue capsules that could be labeled using the mAb against Grl3p (Supplemental Figure S3A). In contrast, Δ*cth3* cells showed no capsule formation and no visibly released mucocyst contents. However, flow cytometric analysis of Δ*cth3* cells before and after stimulation indicated that stimulation did result in some loss of Grl3p staining in the cells (Supplemental Figure S3B). Taken together, these results suggest that Δ*cth3* cells assemble few, if any, exocytosis-competent mucocysts and indicate that *CTH3* plays a key role in mucocyst formation.

CTH3 is required for Grl proprotein processing

Pro-Grl proteins undergo cleavage, and their products assemble to form the dense mucocyst core (Verbsky and Turkewitz, 1998). To ask whether Cth3p was involved in this process, we analyzed cell lysates by Western blotting using anti-Grl antisera. In wild-type cells, Grl1p accumulates primarily as a polypeptide that migrates at ~40 kDa (Figure 7A, lane 2). This product is generated by proteolytic processing from an ~60-kDa proprotein (Ding *et al.*, 1991; Turkewitz *et al.*, 1991). The proprotein is the major species in SB281, a Mendelian mutant that lacks mucocysts and fails to convert the 60 to the 40-kDa form (Orias *et al.*, 1983; Bowman and Turkewitz, 2001; Figure 7A, lane 1). Strikingly, Δ*cth3* lysates showed almost complete absence of the processed Grl1p product and overaccumulation of the precursor (Figure 7A, lane 3). Moreover, parallel Western blots using antibodies against three other proteins in the Grl family yielded similar results (Figure 7, B–D), indicating that Cth3p is required for processing of multiple pro-Grl proteins. No defect in processing of any Grl proproteins was visible in Δ*car1* lysates (Figure 7, lane 4 in each case).

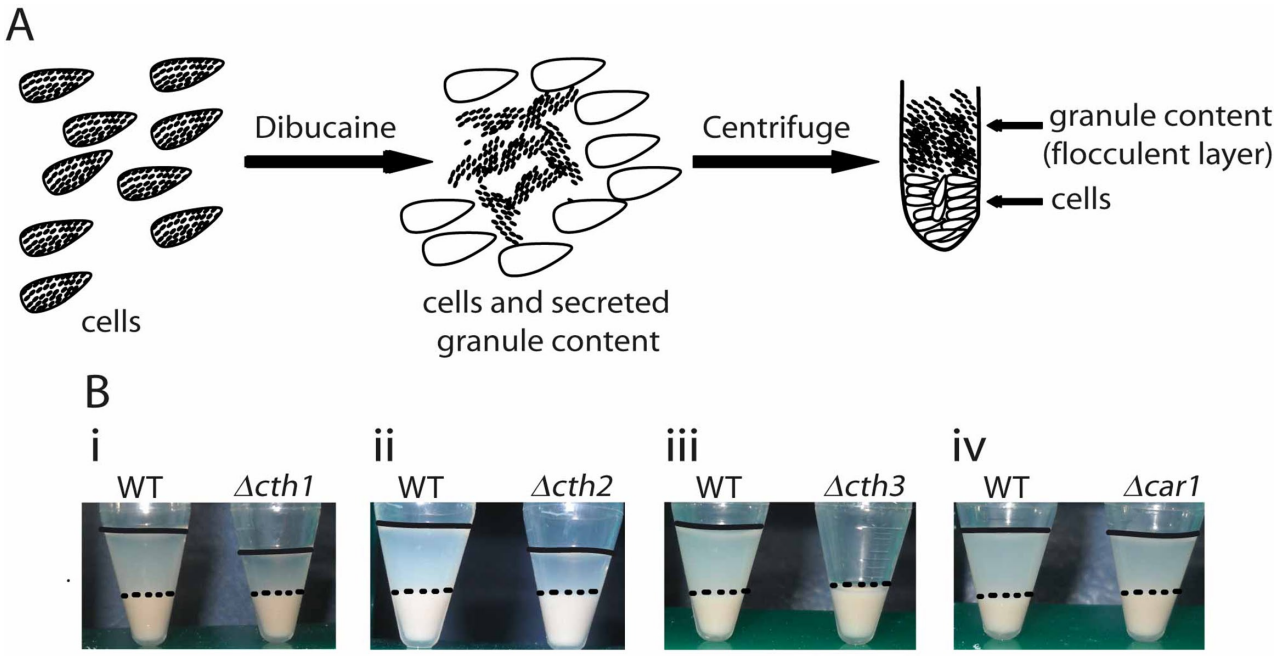

FIGURE 4: The Δ*cth* mutants show reduced release of mucocyst contents. (A) Cartoon representing a semiquantitative assay for mucocyst discharge. Cells are stimulated with dibucaine for 20 s, which triggers regulated exocytosis of mucocyst contents. Subsequent centrifugation results in a dense pellet of cells, with an overlying flocculent composed of expanded dense cores of exocytosed mucocysts. (B) Four independent stimulated wild-type (WT) cell cultures generate the expected two-layered pellet (i–iv, left). For clarity, the flocculent layer in this and all samples are delineated with a dashed line at the lower border and an unbroken line at the upper border. Stimulated Δ*car1* cells produce a flocculent layer identical to wild type (iv, right). Stimulated Δ*cth1-2* cultures show a cell pellet equivalent to WT but a reduced volume of the mucocyst-derived flocculent (i and ii, right). Stimulated Δ*cth3* cells show the most extreme secretion defect and produce no visible flocculent layer (iii, right).

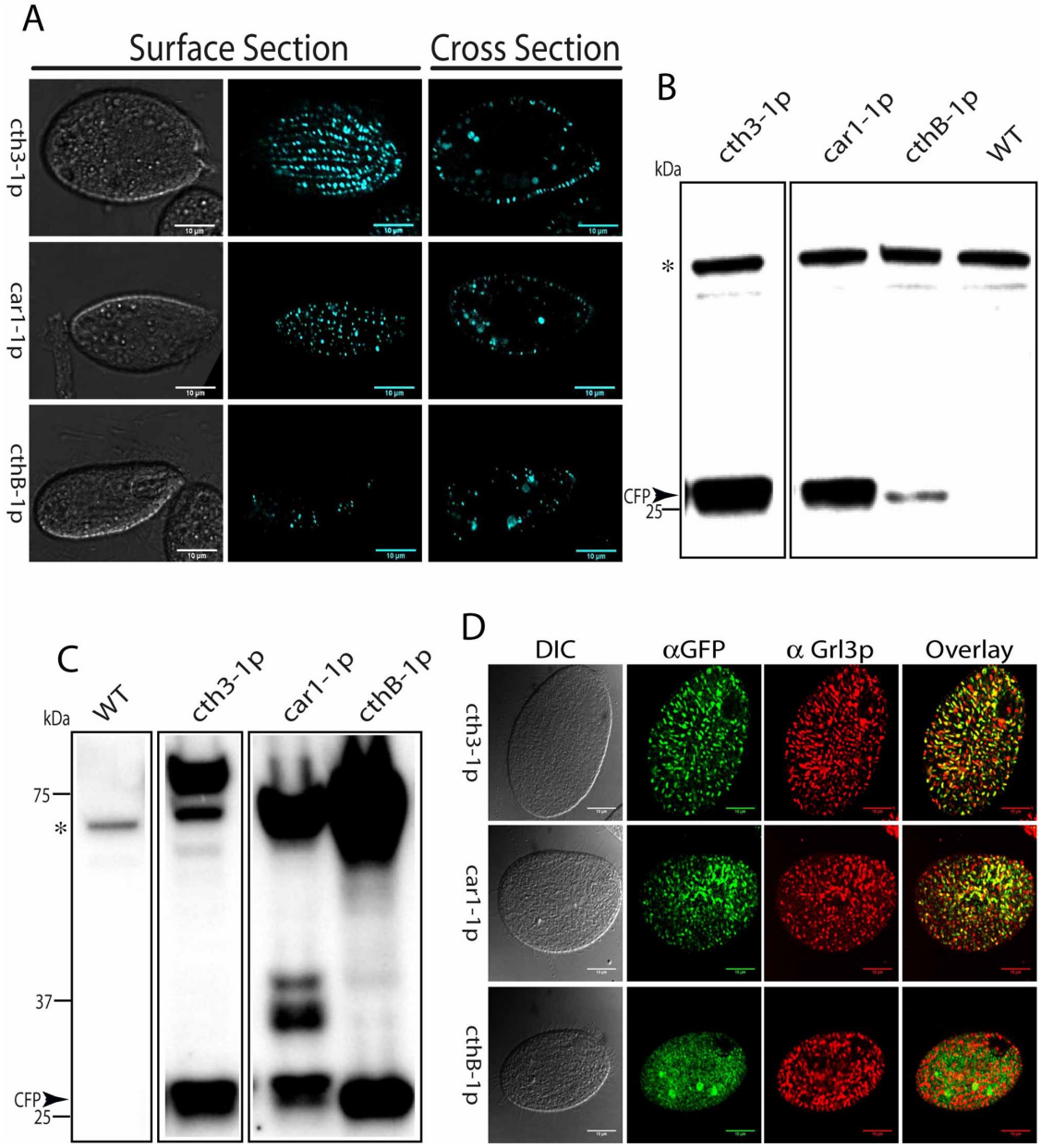

FIGURE 5: Expression and localization of CFP-tagged proteases. (A) Cells expressing CFP-tagged proteases in optical surface and cross sections (left and right, respectively). Bar, 10 μm. Transgene induction was for 16 h with 1 μg/ml $CdCl_2$ at 30°C, followed by 0.2 μg/ml $CdCl_2$ for 4 h in 10 mM Tris, pH 7.4, at 22°C. In cells expressing car1p-CFP (car1-1p) or cth3p-CFP (cth3-1p), the linear arrays of fluorescent puncta at the cell surface correspond to docked mucocysts, which appear as elongated vesicles in cross sections of the same cells. In contrast, cells expressing cthB-CFP (cthB-1p) do not show organized cell surface puncta. (B) Western blot, probed with anti-GFP mAb that cross-reacts with CFP, of lysates of cells shown in A (16 + 4-h transgene induction). Proteins fractions were separated by 4–20% SDS–PAGE and transferred to PVDF before antibody blotting. Molecular weight standards are shown on the left. The only specific band recognized by the antibody, indicated by the arrowhead, is of the size expected for monomeric CFP. A nonspecific species is marked by an asterisk. (C) Western blot as in B, but in which transgene expression in the same cell lines was induced for just 2 h with 1 μg/ml $CdCl_2$. The strongest antibody-reactive bands correspond to the predicted molecular weights of the tagged proteins: Cth3p-CFP, 78 kDa; Car1p-CFP, 67 kDa; and CthB-CFP, 65 kDa. A nonspecific species is marked by an asterisk. (D) Cells after 2 h of transgene induction (as in C) were fixed and immunolabeled with mouse monoclonal antibody mAb 5E9 to localize the mucocyst protein Grl3p and rabbit anti GFP Ab to localize the protease-CFP fusions. In cells expressing cth3-1p and car1-1p, there is extensive overlap between CFP and Grl3p immunolocalization, whereas no colocalization is seen between cthB-1p and Grl3p. Images are single slices, for clarity. The apparent difference in cell size between samples is due to variable flattening by the coverslips.

To confirm that the observed defects in the Δ*cth3* are due to disruption of *CTH3* itself rather than perturbation of expression from nearby loci, we introduced into the Δ*cth3* cells a copy of the *CTH3* open reading frame (ORF), fused to CFP and integrated at the *RPL29* locus and under the control of the inducible *MTT1* promoter, to generate strain *cth3-2p*. Expression of the predicted fusion

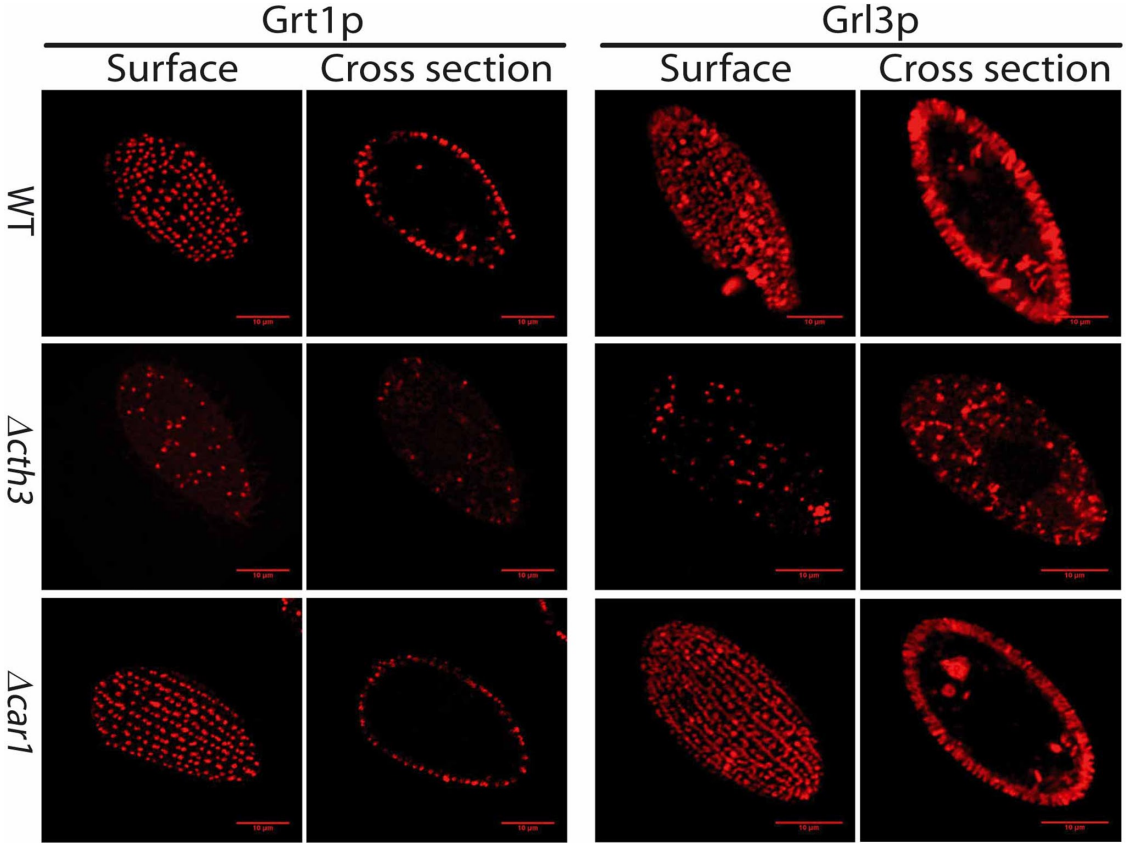

FIGURE 6: *CTH3* is required for DCG formation. Top, docked mucocysts in fixed wild-type cells, immunolabeled using mAb 4D11 that recognizes Grt1p (left two), and mAb 5E9 that recognizes Grl3p (right two). Surface and cross sections. Middle, parallel immunostaining of Δ*cth3* cells shows little or no mucocyst signal. The low level of Grt1p signal is concentrated at the cell periphery, whereas the majority of the Grl3p signal is found in cytoplasmic puncta. Bottom, parallel immunostaining of Δ*car1* cells shows a pattern indistinguishable from wild type. Scale bars, 10 μm.

protein in this strain was detected by Western blot (Supplemental Figure S4A) and localized to mucocysts by anti–green fluorescent protein (GFP) antibody staining (Supplemental Figure S4C). As discussed for the case of overexpressed tagged Cth3p, prolonged induction led to the appearance of monomeric CFP, consistent with endoproteolytic processing (Supplemental Figure S4B). Of importance, expression of Cth3p-CFP rescued the mucocyst biosynthesis defect (Supplemental Figure S4D), as well as pro-Grl1p processing (Supplemental Figure S4E), in the Δ*cth3* cells. These results support the idea that Cth3p is a key factor in pro-Grl processing. Together with other data described later, these results also indicate that fusions between Cth3p and fluorescent proteins (CFP, GFP) retain enzymatic activity.

CTH3 expression suppresses the pro-Grl processing defect in a nonallelic mutant

Tetrahymena mutants with defects in mucocyst assembly or exocytosis have been isolated after nitrosoguanidine mutagenesis (Orias *et al.*, 1983; Melia *et al.*, 1998; Bowman *et al.*, 2005a). A large subset was found to have defects in pro-Grl processing, although it is not yet known in any case whether this represents the primary defect. The mutant with the most severe defect in pro-Grl processing is SB281, mentioned earlier, which shows neither detectible pro-Grl processing nor mucocyst formation (Bowman and Turkewitz, 2001). The SB281 mutation cannot fall within *CTH3*, since SB281 has been genetically mapped to micronuclear chromosome 4, whereas the *CTH3* gene is on chromosome 5 (Gutierrez and Orias, 1992; E. Hamilton, personal communication). Nonetheless, it seemed possible that overexpression of *CTH3* could suppress the SB281 defect. To test this, we integrated the wild-type *CTH3* open reading frame, including a C-terminal hexahistidine (6xHis) epitope tag, at the *RPL29* locus in SB281 cells, under the control of the inducible *MTT1* promoter. High-level expression of Cth3p partially rescued the SB281 pro-Grl processing defect (Supplemental Figure S5, A and B). Of interest, the distribution of a putative Cth3p substrate, the mucocyst core protein Grl3p, was also affected by expression of cth3p-6xHis in SB281 cells. In growing SB281 cells, Grl3p is found in large, heterogeneous cytoplasmic puncta (Supplemental Figure S5, C and D, top row). SB281 transformed to overexpress cth3p-6xHis still contains Grl3p-positive, large, heterogeneous structures, but in addition contains abundant smaller and more homogeneous Grl3p-positive puncta (Supplemental Figure S5D, bottom row). These do not have the elongated shape of mucocysts and are unlikely to represent viable mucocyst intermediates since they do not contain a second mucocyst core marker, Grt1p, whose distribution in SB281 cells is unchanged by overexpression of Cth3p (Supplemental Figure S5E). As pointed out earlier, Grt1p is not processed and therefore not a potential substrate for Cth3p. Thus the overexpression of Cth3p in SB281 cells leads to both processing and redistribution of Grl3p, suggesting that Grl processing is a key step in driving reorganization of core proteins during mucocyst formation.

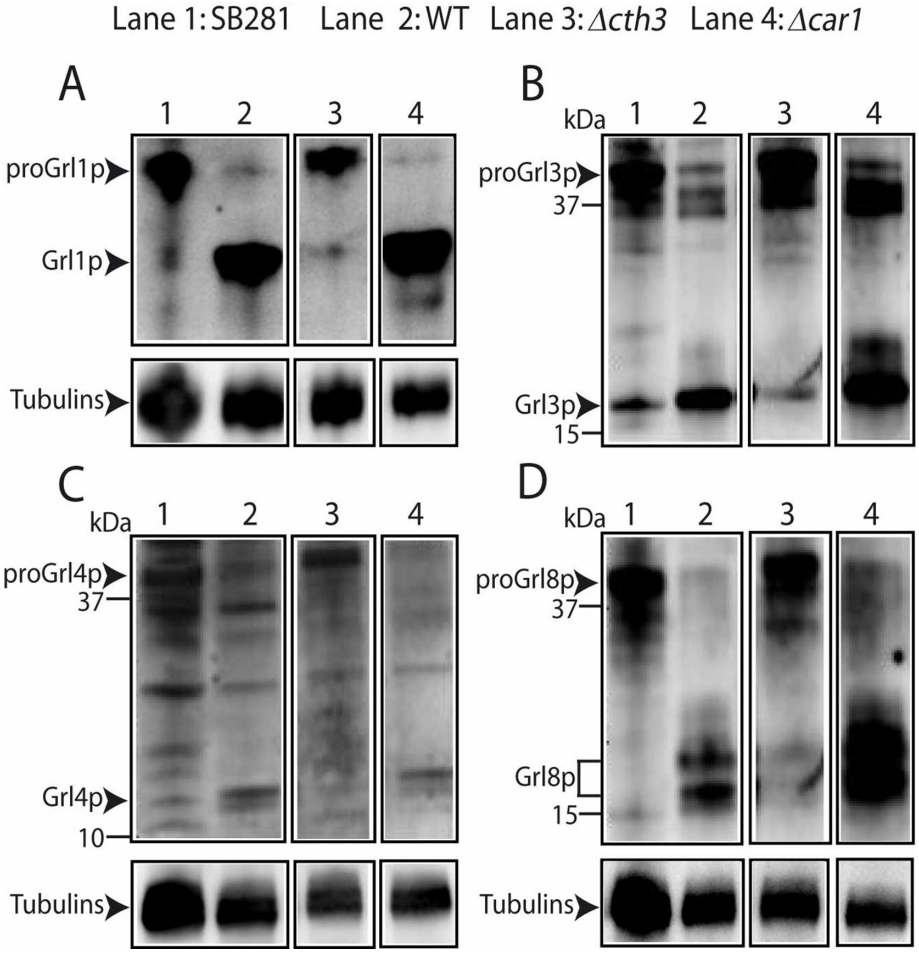

FIGURE 7: *CTH3* is required for processing of proGrl proteins. Cell lysates (5000 cell equivalents in A, 10,000 cell equivalents in B–D) were resolved by SDS–PAGE, transferred to PVDF, and Western blotted with antibodies against mucocyst proteins in the GRL family, all of which undergo proteolytic processing in wild-type cells during formation of the mucocyst dense core. The SB281 mutant is blocked in both mucocyst formation and proGrl processing. (A) Blotting with anti-Grl1p antibody. Wild type and Δ*car1* (lanes 2 and 4) show primarily the mature processed Grl1p product, and SB281 and Δ*cth3* (lanes 1 and 3) show primarily the unprocessed precursor. An anti-tubulin antibody was used to control for loading. (B) Same as A, but blotting with anti-Grl3p antibody. (C) Same as A, but blotting with anti-Grl4p antibody. (D) Same as A, but blotting with anti-Grl8p antibody. B is a reprobe of stripped result in D, so the loading controls in D apply to both. In all cases, the unprocessed (proGrl) and processed (Grl) species are indicated.

Cth3p activity in vivo and in vitro depends on the conserved catalytic residues

The role of *CTH3* in mucocyst maturation is likely to require its predicted enzymatic activity. To test this idea, we used homologous recombination to replace endogenous *CTH3* in the macronucleus of wild-type cells either with itself (*cth3-4*) or with a variant in which we made mutations in both conserved catalytic motifs (Asp139 to Asn; Asp324 to Asn; *cth3-5*). These mutations have been shown in other systems to cripple the activities of homologous cathepsins (Tyynela *et al.*, 2000; Glondu *et al.*, 2001). In both cases, the replacement allele included a C-terminal fusion to GFP (Figure 8A), and transformants were passaged extensively in selective media to drive the replacement alleles to fixation or near fixation. Western blotting of whole-cell lysates using an anti-GFP antibody indicated that the expected fusion protein was synthesized in each strain (Figure 8B). In addition, a minor band of the size expected for monomeric GFP was present, suggesting that some endoproteolytic cleavage of the fusion proteins had occurred. Of interest, monomeric GFP was present both in cells expressing the enzymatically active cth3-4p and in the enzymatically disabled cth3-5p, although it was more abundant in the former (Figure 8B). In cells expressing cth3-4p, both the fusion protein and monomeric GFP were secreted into the cell culture medium, but neither species was secreted in cells expressing the enzymatically disabled cth3-5p (Supplemental Figure S6A).

Of importance, cells expressing cth3-5p were indistinguishable from Δ*cth3* in their failure to process proGrl1p (Figure 8C) or to release mucocyst contents on stimulation (Figure 8D). Indeed, like Δ*cth3* cells, the *cth3-5* cells fail to synthesize Grl3p-positive mucocysts (Figure 8E, middle row). In contrast, cells expressing cth3-4p were indistinguishable from wild type in proprotein processing and mucocyst synthesis and exocytosis. The GFP signal in cells expressing cth3-4p accumulated in mucocysts (Figure 8F, bottom row), as expected. In contrast, the GFP signal in cells expressing cth3-5p accumulated in heterogeneous cytoplasmic puncta (Figure 8F, middle row). This difference could also be seen via live imaging of the same cultures (Supplemental Figure S6B). Taken together, these results strongly support the conclusion that the key role of Cth3p in mucocyst biogenesis depends on its enzymatic activity. Consistent with this conclusion, the expression of a catalytically disabled *CTH3* variant from the *RPL29* locus in Δ*cth3* cells failed to rescue any of the Δ*cth3* defects (Supplemental Figure S7).

To demonstrate more directly that Cth3p possesses enzymatic activity, we used anti-GFP antibodies to immunoprecipitate cth--4p and cth3-5p from detergent lysates of *Tetrahymena* expressing these constructs. The immunoprecipitates, adjusted for yield differences for the two proteins, were then assayed for activity against a fluorogenic cathepsin D substrate (Figure 8, G and H). Cth3-4p, but not cth3-5p, displayed clear activity in this assay, consistent with and confirming the in vivo results.

Cth3p partially colocalizes with both endosomal and lysosomal probes

As detailed earlier, whereas cth3p-GFP colocalizes strongly with the mucocyst marker Grl3p, there is also significant GFP signal in nonmucocyst structures, as judged by their morphology and distribution. These nonmucocyst structures are relatively prominent in high-density cultures but almost undetectable in low-density cultures (Figure 9A). Some of these structures may be intermediates in mucocyst maturation, including compartments involved in the delivery of processing enzymes to immature mucocysts. In addition, Cth3p may play roles unrelated to mucocyst formation, since one would not expect a gene dedicated to mucocysts to have a growth phenotype.

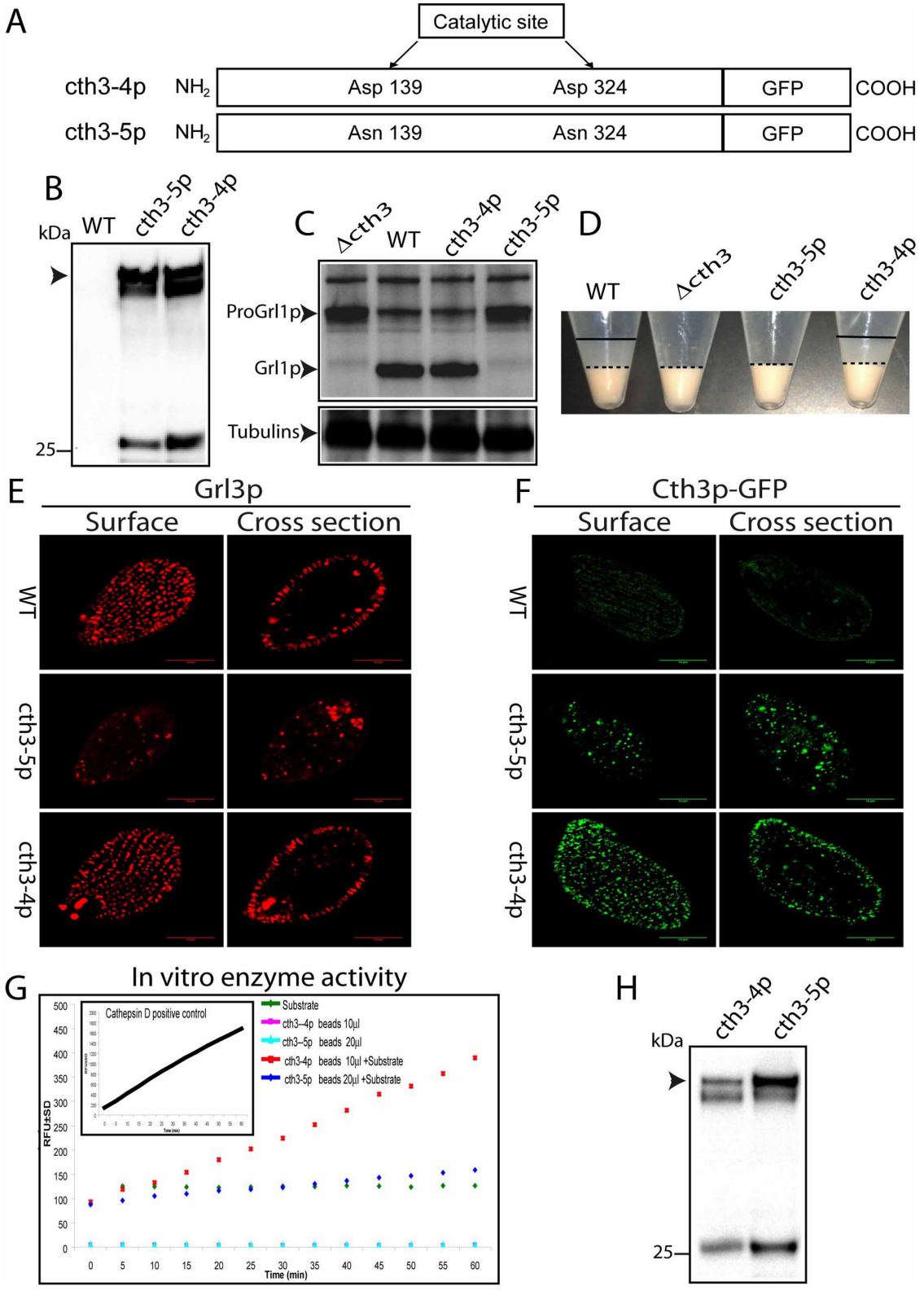

FIGURE 8: Mucocyst formation, proGRL processing, and in vitro enzymatic activity require the conserved active-site residues in Cth3p. (A) Schematic representation of wild-type and mutant Cth3p, both with C-terminal GFP tags, showing locations of mutations to change Asp → Asn at the two predicted catalytic sites. (B) Expression of GFP-tagged and Asp → Asn, GFP-tagged constructs (*cth3-4* and *cth3-5*, respectively). Constructs were expressed at the native *CTH3* locus as gene replacements. Fusion proteins were immunoprecipitated from detergent lysates using polyclonal rabbit anti-GFP antiserum. Immunoprecipitates were subjected to SDS–PAGE, and PVDF transfers were blotted with monoclonal anti-GFP Ab. Both of the transformed cell lines, but not wild type, show immunoreactive bands of the size expected for the Cth3p-GFP fusion, as well as a band likely to correspond to monomeric GFP. (C) The proGrl processing in wild-type

To gain some insight into the nature of the cth3p-GFP-positive structures, we incubated cells expressing cth3p-GFP from the endogenous locus with LysoTracker Red (Figure 9B). Consistent with previous studies, docked mature mucocysts did not stain with the LysoTracker probe (Bright *et al.*, 2010). Simultaneous imaging in the red and green channels showed that the majority of LysoTracker-positive structures also contained cth3p-GFP. Some structures appear to consist of a LysoTracker-positive zone tightly apposed to the cth3p-GFP-positive zone, suggesting that a fraction of cth3p-GFP resides in an organelle that communicates with lysosomes.

To ask whether Cth3p localized to endosomes, we incubated cth3p-GFP-expressing cells with FM4-64, which was previously used in this system to label endosomes derived from clathrin-coated vesicles (Elde *et al.*, 2005). At a variety of chase times after an initial pulse of FM4-64, we observed multiple structures showing near colocalization of FM4-64 and cth3p-GFP (Figure 9C). Taken together, the results support the idea that Cth3p is associated with the endolysosomal pathway.

The partial localization of Cth3p to an endosomal compartment led us to ask whether the enzyme could be delivered to that compartment via endocytosis. If so, this might provide an experimental approach to resolving the hypothesized distinct functions of Cth3p. We therefore tested whether any phenotypes in Δ*cth3* cells might be suppressed by incubating the cells in medium containing Cth3p. As shown earlier, Cth3p is found in the medium of wild-type cells. Remarkably, we found that the Δ*cth3* growth phenotype could be suppressed, and in a concentration-dependent manner, by growing cells in medium previously harboring either wild-type cells or cells that were overexpressing cth3p-CFP but not in medium from Δ*cth3* cultures (Figure S8, A–C). However, there was no detectible rescue of pro-Grl processing or mucocyst formation in these cultures (unpublished data). We hypothesize that the endolysosomal activity of Cth3p is essential for rapid growth, and this pool of enzyme can be provided via endocytosis, but proGrl processing occurs in a different compartment that is either less accessible via endocytosis or requires a higher concentration of enzyme.

DISCUSSION

Pioneering molecular studies on dense-core granule formation in ciliates, conducted more than three decades ago, implicated proteolytic processing of core proteins in generating the elaborate structures (Collins and Wilhelm, 1981; Adoutte *et al.*, 1984). Subsequent identification of the core proteins, and in particular the chemical analysis of their processed forms, led to inferences about target-site specificity and how differential affinity of proteases for their substrates might control assembly of the granule core (Gautier *et al.*, 1996; Verbsky and Turkewitz, 1998; Vayssie *et al.*, 2001). Although some inferences could be tested by site-specific mutagenesis of deduced processing sites (Bradshaw *et al.*, 2003), the models were limited by the lack of any direct information on the proteases themselves.

Here we used expression profiling in *T. thermophila* to identify a set of likely candidates for the mucocyst-processing enzymes. Transcriptional profiling has been a useful tool in other systems, in particular mammalian tissue culture cells, to identify genes associated with some pathways of membrane traffic (Gurkan *et al.*, 2005). Expression profiling in *T. thermophila* is greatly facilitated by an online database of gene expression over a wide range of culture conditions (Miao *et al.*, 2009; Xiong *et al.*, 2011, 2013). Since its creation, the database has helped to link a number of genes with distinct cellular processes (Bright *et al.*, 2010; Stover and Rice, 2011; Nusblat *et al.*, 2012; Xu *et al.*, 2012).

The *T. thermophila* genome is laden with predicted proteases (Eisen *et al.*, 2006). However, we found that only five of these had transcriptional profiles matching those of the *GRL* genes. Because the GRL proteins undergo obligatory cleavage during mucocyst formation, the five proteases appeared as strong candidates for enzymes involved in this process. These comprised three predicted aspartyl cathepsins (*CTH1–3*), a cysteine cathepsin (*CTH4*), and a carboxypeptidase (*CAR1*). Each of these proteins, CFP tagged at the carboxy terminus, showed clear targeting to docked mucocysts. Localization to mucocysts is likely to be due to specific sorting signals rather than default, since GFP linked to an N-terminal endoplasmic reticulum translocation sequence does not localize to mucocysts (Haddad *et al.*, 2002; Bowman *et al.*, 2005a). For a subset of proteins, targeting to mucocysts may be receptor mediated. One of the candidate proteases, Cth3p, was previously shown to undergo significant mislocalization in cells lacking a sortilin/VPS10-family receptor, *SOR4* (Briguglio *et al.*, 2013).

The genes encoding the three aspartyl proteases and the sole carboxypeptidase were each targeted for disruption via homologous recombination in the somatic macronucleus. The prediction,

and mutant cell lines. Cell lysates (10^4 cell equivalents) were separated by SDS–PAGE and blotted with anti-Grl1p antibody, as in Figure 7. Wild-type and *cth3-4* cells accumulate processed Grl1p. In contrast, Δ*cth3* cells and *cth3-5* cells accumulate proGrl1p. (D) The mucocyst discharge assay shown in Figure 4 was performed on cell lines analyzed in C. Wild-type cells and cells expressing cth3-4p release a flocculent layer (between the solid and broken lines) after stimulation with secretagogue, whereas Δ*cth3* cells and cells expressing cth3-5p show no release upon stimulation. (E, F) Immunostaining of fixed cells, as in Figure 5D, to visualize mucocyst protein Grl3p and GFP-fusion proteins. In E, wild-type cells and cells expressing cth3-4p show the expected pattern of Grl3p in docked mucocysts, whereas cells expressing cth3-5p show chiefly cytoplasmic puncta. In F, wild-type cells show background signal, whereas cells expressing cth3-4p show labeling consistent with extensive localization of the GFP-fusion protease to mucocysts. In contrast, cth3-5p localizes largely in cytoplasmic puncta. Scale bars, 10 μm. Enzymatic activity of purified Cth3p. (G) Cell cultures, 150 ml, of *T. thermophila* expressing cth3-4p or cth3-5p (3×10^5/ml) were washed and solubilized with detergent, and GFP-tagged fusion proteins were immunoprecipitated using bead-coupled polyclonal rabbit anti-GFP antiserum. After extensive washing, beads were resuspended in assay buffer as described in *Materials and Methods*. To compensate roughly for the difference in immunoprecipitation yields between cth3-4p and cth3-5p, the bead volume used for the former was half that used for that latter (10 vs. 20 μl) in a total reaction volume of 100 μl. The results are plotted as relative fluorescence units (RFU) ± SD vs. time. Bovine cathepsin D (10 ng) was assayed in parallel as a positive control (inset). (H) SDS–PAGE and Western blotting, using anti-GFP mAb, of IP preparations (10 μl of cth3-4p and 20 μl of cth3-5p beads) assayed in G.

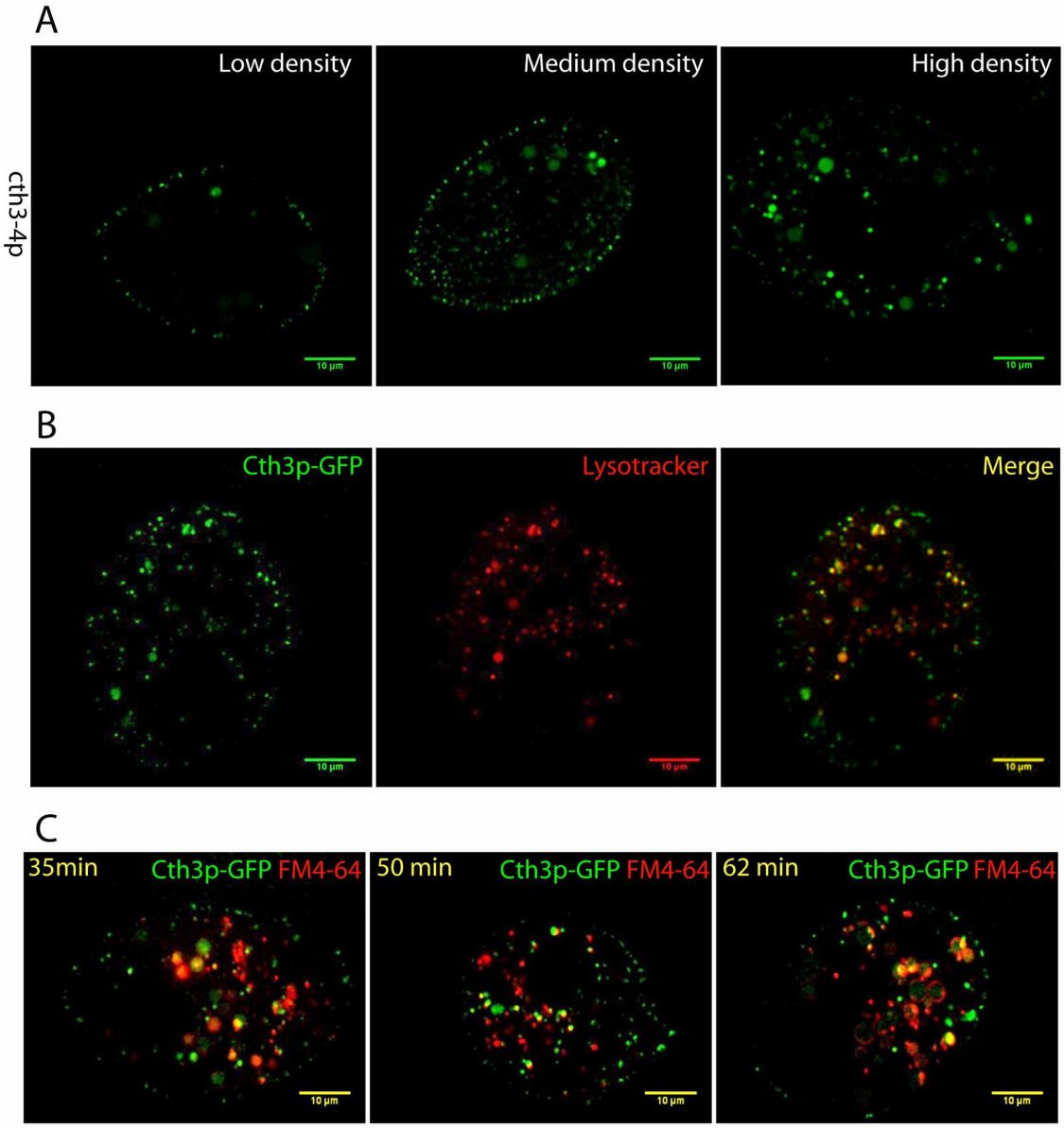

FIGURE 9: Non–mucocyst-localized Cth3p shows some overlap with endosomal and lysosomal markers. In all cases, cth3p-GFP (cth3-4p) is expressed at the native *CTH3* locus, and GFP autofluorescence was imaged in live cells. Optical sections shown are cell cross sections. (A) Cth3p shows variable localization, depending on cell culture density. Cell cultures were sampled at low ([1–1.5] $\times$ 10^5/ml), medium ([2.5–3.5] $\times$ 10^5/ml) and high ([5–6.5] $\times$ 10^5/ml) density. An increasing number of heterogeneous cytoplasmic puncta are seen in cells from denser cultures. (B) Cells from a culture at 6 $\times$ 10^5/ml were incubated for 5 min with 200 nM LysoTracker. Live images were captured within 30 min after addition of LysoTracker. (C) Cells from a culture at 6 $\times$ 10^5/ml were incubated for 5 min with 5 μM FM4-64, which labels endosomes, and then pelleted and resuspended in fresh medium. The times shown represent minutes postresuspension. Scale bars, 10 μm.

implied but never directly tested in ciliates, was that inhibition of processing during granule assembly would compromise the efficiency of exocytosis, since extrusion of granule contents depends on rapid expansion of the precisely assembled core. Each of the cathepsin disruption strains showed a deficit in exocytosis as measured by a semiquantitative release assay, whereas the carboxypeptidase (*CAR1*)-knockout strain had a wild-type secretory response. The absence of an exocytosis phenotype in Δ*car1* cells may suggest that carboxy-terminal trimming is not essential for assembling the expansible mucocyst core but instead plays another role, which may be related to the activity of the mucocyst contents post release. Those activities are poorly understood for *T. thermophila* in particular and for ciliates in general. The Δ*cth1* and Δ*cth2* strains each showed a modest exocytic deficit. Although those genes are not closely related, it is possible that they may have overlapping activities, which can be explored by engineering a double *cth1/cth2* knockout. Disruption of *CTH3* resulted in cells with no detectible exocytic release.

The Δ*cth3* cells were similar to a previously characterized Mendelian mutant that lacks mucocysts, called SB281 (Orias *et al.*, 1983). Like SB281, the Δ*cth3* cells showed little or no processing of pro-Grl proteins that are cleaved during mucocyst maturation, but instead

they accumulated the Grl precursors in large, heterogeneous cytoplasmic puncta (Bowman and Turkewitz, 2001). The small number of docked mucocysts that accumulate in Δ*cth3* cells may be accounted for by the fact that we could not disrupt all macronuclear copies of the apparently essential *CTH3* gene.

Significantly, Δ*cth3* cells are deficient in the processing of all Grl proteins tested. Moreover, the size of the accumulated precursors suggests that none of the endoproteolytic cleavage events inferred in previous studies takes place in the absence of Cth3p. These defects have also been noted in the SB281 mutant, but prior analysis indicated that the primary defect in SB281 was unlikely to be at the level of proprotein processing (Bowman and Turkewitz, 2001). The genetic lesion in SB281 maps to chromosome 4, whereas *CTH3* lies on chromosome 5 (Gutierrez and Orias, 1992; E. Hamilton, personal communication). We found that overexpression of Cth3p in SB281 can partially suppress the proGrl processing defect. Of most interest, these partially rescued cells also show a change in the appearance of cytoplasmic Grl3p-positive puncta, consistent with the idea that proprotein processing drives reorganization of the granule core proteins, as seen in other systems that depend on unrelated proteases and core proteins (Bendayan, 1989). Cth3p may also have non-Grl substrates that could contribute to the noted phenotypes. However, we found that overexpression of Cth3p in SB281 did not change the distribution of Grt1p, a nonprocessed mucocyst protein. This suggests that Cth3p overexpression acts directly on Grl proteins or on a step that affects them but not proteins in the Grt family.

Based on sequence analysis, *CTH3* belongs to the aspartyl cathepsin superfamily. We found that purified Cth3p-GFP cleaves a canonical cathepsin D substrate, and this activity was lost when the two predicted active-site residues were mutated. We tested the importance of enzymatic activity in vivo by asking whether the role of Cth3p in mucocyst synthesis depended on those active-site residues. Replacement of endogenous *CTH3* with a GFP-tagged but otherwise wild-type copy resulted in cells with normal mucocyst accumulation, exocytosis, and pro-Grl processing. In contrast, replacement with a copy of *CTH3* with single–amino acid mutations at the two predicted active sites resulted in cells that showed all the defects of Δ*cth3*. These results strongly support the hypothesis that Cth3p is a key processing enzyme during mucocyst formation. We hypothesize that Cth3p acts directly on proGrl substrates but cannot rule out the possibility that Cth3p acts, in addition or exclusively, to activate proteases that in turn are directly responsible for proGrl processing. These may include other aspartyl and/or cathepsin proteases identified in the expression-based screen. Proteolytic activation of proteases is well documented in many lineages, including the sister lineage to the ciliates, the apicomplexans, in which compartment-specific activation of zymogens is important for secretory organelle formation (Dou and Carruthers, 2011; Dou *et al.*, 2013). Our data argue against the idea that any of the other enzymes identified in our screen is required for Cth3p activation, since no other gene knockout (including *CTH4*; unpublished data) conferred a phenotype comparable to Δ*cth3*.

Surprisingly, *CTH3* may be important for growth, since prolonged selection to disrupt all macronuclear copies of the gene resulted in multiple independent clones that retained detectible *CTH3* transcript and grew more slowly than wild type. In contrast, the Δ*cth1* and Δ*cth2* grew at wild-type rates. Remarkably, the growth phenotype in Δ*cth3* was suppressed for multiple clones when the mutant cells were grown in medium conditioned by cells expressing (or overexpressing) *CTH3*. We hypothesize that the active factor in the medium is Cth3p itself, which is secreted from wild-type cells and might be taken up via receptor-mediated endocytosis involving sortilin receptors (Briguglio *et al.*, 2013). The result suggests that Cth3p activity in an endosomal compartment is required for rapid growth. Localization of Cth3p in endosomes is also consistent with our localization data, although the precise identity of the compartments remains to be established. Our results do not imply that endocytic uptake of Cth3p occurs in free-living *T. thermophila*, since these may generally exist at much lower densities than in laboratory cultures. The growth rescue is unlikely to be linked with the role of *CTH3* in mucocyst formation, since mucocysts are dispensable for laboratory growth of *T. thermophila*; for example, SB281 shows no growth defect. Moreover, Δ*cth3* cells grown in conditioned medium showed no rescue of pro-Grl processing or mucocyst formation. However, our results do not rule out the possibility that some direct or indirect product of Cth3p activity, rather than Cth3p itself, is responsible for the growth rescue.

Cth3p is related to a group of cathepsins in ciliates and apicomplexans and more distantly related to cathepsins in other eukaryotes. The precise relatedness is unsettled, given the low bootstrap values in the phylogenetic reconstruction, which are typical of fast-evolving ciliate genes (Zufall *et al.*, 2006). The related animal cathepsins have chiefly been characterized as endolysosomal enzymes (Zaidi *et al.*, 2008), which appears consistent with our localization data on Cth3p and may explain the unexpected growth phenotype. Aspartyl cathepsins have also been implicated in proprotein processing of mammalian granule proteins (Krieger and Hook, 1992).

In *Tetrahymena*, the extensive colocalization of Cth3p-GFP and Grl3p, together with other data, argues that Cth3p is primarily found in mucocysts or mucocyst intermediates and therefore suggests that the retargeting of an endolysosomal enzyme was a critical step in the evolution of secretory granules in ciliates. Of interest, distantly related cathepsins in mammals have been implicated in proprotein processing in secretory granules (Hook *et al.*, 2004). We also found Cth3p in cell culture supernatants but not in supernatants of cells expressing an enzymatically disabled Cth3p variant. These results can be explained if Cth3p is secreted from wild-type cells via mucocyst exocytosis, which may occur at low levels in unstimulated cultures. In cells expressing enzymatically inactive Cth3p there are no mucocysts and hence no Cth3p secretion, and the protein may instead be degraded. Wild-type *T. thermophila* secretes a variety of hydrolases via secretory lysosomes (Kiy *et al.*, 1993). Of importance, such lysosomes can be clearly distinguished from mucocysts, in part based on analysis of Mendelian mutants that affect one or the other pathway (Hunseler and Tiedtke, 1992; Melia *et al.*, 1998). If *Tetrahymena* secrete Cth3p via mucocysts, an interesting question is whether there are different physiological consequences to secreting proteases via one route versus another.

A particularly interesting group of cathepsins to consider for potential insight into the evolution and function of the *T. thermophila* enzymes are those in the sister lineage to ciliates, the apicomplexans. The apicomplexan parasite *Toxoplasma gondii* contains complex secretory organelles whose formation, like that of mucocysts in *Tetrahymena*, requires the activity of multiple proteases. These *Toxoplasma* proteases have received attention as potential therapeutic targets because the secretory organelles are required for host cell invasion (McKerrow, 1999; Que *et al.*, 2002, 2007). Of interest, all cathepsins known to be involved in *T. gondii* belong to the cysteine cathepsin subfamily and are therefore more closely related to *T. thermophila CTH4* and cathepsin B than to *CTH3* (Que *et al.*, 2002). *T. gondii* encodes seven aspartyl cathepsins, not all of which have been characterized, but the three most closely related to *T. thermophila CTH3* do not appear to have roles in secretory

Strain name	Phenotype	Details of relevant genetic modification	Source
B2086	Wild type	None	J. Gaertig (University of Georgia, Athens, GA)
CU428	Wild type	None	P. Bruns (Cornell University, Ithaca, NY)
SB281	No mucocysts; no processing of mucocyst proproteins	Nitrosoguanidine-induced Mendelian mutant	E. Orias (University of California, Santa Barbara, Santa Barbara, CA)
UC801	Δ*cth1*; >10-fold knockdown of *CTH1* expression	Replaces nucleotides –34–925 of macronuclear *CTH1* ORF with NEO4 cassette	This study
UC802	Δ*cth2*; >10-fold knockdown of *CTH2* expression	Replaces nucleotides 1–922 of macronuclear *CTH2* ORF with NEO4 cassette	This study
UC803	Δ*cth3*; >10-fold knockdown of *CTH3* expression	Replaces nucleotides –23–991 of macronuclear *CTH3* ORF with NEO4 cassette	This study
UC804	Δ*car1*; no detectible *CAR1* expression	Replaces nucleotides –86–858 of macronuclear *CAR1* ORF with NEO4 cassette	This study
Not stable cell line	High-level inducible expression of CFP-tagged Cth3p (cth3-1p)	C-terminal fusion of Cth3p and CFP, expressed under the control of the *MTT1* promoter, on the multicopy rDNA minichromosome	This study
Not stable cell line	High-level inducible expression of CFP-tagged CthB (cthB-1p)	C-terminal fusion of CthB and CFP, expressed under the control of the *MTT1* promoter, on the multicopy rDNA minichromosome	This study
Not stable cell line	High-level inducible expression of CFP-tagged Car1p (car1-1p)	C-terminal fusion of Car1p and CFP, expressed under the control of the *MTT1* promoter, on the multicopy rDNA minichromosome	This study
UC805	Inducible expression of CFP-tagged Cth3p (cth3-2p)	C-terminal fusion of Cth3p and CFP, expressed under the control of the *MTT1* promoter, at the macronuclear *RPL29* locus of Δ*cth3* (UC803)	This study
UC806	Inducible expression of enzymatically disabled, CFP-tagged Cth3p (cth3-3p), in a Δ*cth3* background	Mutated variant of *CTH3* (Asp139 → Asn; Asp324 → Asn), C-terminally fused to CFP and under the control of the *MTT1* promoter, integrated at macronuclear *RPL29* locus of Δ*cth3* (UC803)	This study
UC807	Endogenous-level expression of GFP-tagged Cth3p (cth3-4p)	C-terminal fusion of Cth3p and GFP, integrated at the macronuclear *CTH3* locus	This study
UC808	Endogenous-level expression of enzymatically disabled, GFP-tagged Cth3p (cth3-5p)	Mutated variant of Cth3p (Asp139 → Asn; Asp324 → Asn), C-terminally fused to GFP, integrated at the macronuclear *CTH3* locus	This study
UC809	Inducible expression of His-tagged Cth3p (cth3p-6xHis)	C-terminal fusion of Cth3p and 6xHis, expressed under the control of the *MTT1* promoter, at the macronuclear *RPL29* locus of SB281	This study

TABLE 1: Description of *Tetrahymena* strains.

organelle formation (Shea *et al.*, 2007). Because secretory organelles are widespread in both ciliates and apicomplexans, a wider sampling in both lineages could support an ancestral role of cysteine, but not aspartyl, proteases in the formation of specialized secretory compartments in this deep lineage.

MATERIALS AND METHODS

Tetrahymena strains and culture conditions

T. thermophila strains CU428, B2086, and SB281 were grown at 30°C with agitation in SPP medium (1% proteose peptone, 0.2% dextrose, 0.1% yeast extract, 0.003% ferric EDTA). All reagents were from Sigma-Aldrich (St. Louis, MO) unless otherwise indicated. Culture densities were measured using a Z1 Coulter Counter (Beckman Coulter, Indianapolis, IN). Cell cultures were analyzed after growing to densities of (2–4) × 10^5 cells/ml unless otherwise indicated. Details of *T. thermophila* strains are given in Table 1.

Expression of cathepsins and carboxypeptidase gene fusions

The Gateway (Invitrogen, Grand Island, NY) system was used to engineer CFP fusions to create cth3-1p, cthB-1p, and car1-1p. Briefly, PCR-amplified *CTH3* (TTHERM_00321680), *CTHB*

(TTHERM_00083480), and *CAR1* (TTHERM_00410180; minus the stop codons) were TOPO cloned (Invitrogen) into the pENTR-D-TOPO entry vector. CACC was added to each forward primer in order to allow directional cloning into pENTR-D. The pENTR clones were sequenced and the genes recombined using the Clonase reaction into the target Gateway-based *T. thermophila* expression vector pICC-GTW, a gift from Doug Chalker (Washington University, St. Louis, MO; Yao *et al.*, 2007; Bright *et al.*, 2010). Genes subcloned into pICC-GTW are fused to the N-terminus of the CFP gene, with the fusion under the transcriptional control of the cadmium-inducible *MTT1* promoter (Shang *et al.*, 2002). When introduced into *Tetrahymena*, the vector is amplified and maintained as a macronuclear minichromosome and confers paromomycin resistance.

Expression of CFP fusions was confirmed by microscopy (see later description) and Western blotting. For the latter, cells were treated with 1 µg/ml $CdCl_2$ for 2 or 16 h. After 16 h of induction, cells were further induced in starvation buffer (10 mM Tris, pH 7.4) containing 0.2 µg/ml $CdCl_2$ at 22°C for 4 h. Samples were then processed for Western blotting, as described later.

Generation of cathepsin- and carboxypeptidase-knockout strains

PCR was used to amplify the *CTH1-3* and *CAR1* upstream regions (1.5–2 kb) and a portion of the ORFs plus downstream flanking regions (1.5–2 kb total), which were subsequently subcloned into the *Sac*I and *Xho*I sites of the neo4 cassette, respectively, using In-Fusion cloning kit (Clontech, Mountain View, CA). The sequences of the primers are listed in Supplemental Table S2. The constructs were linearized by digestion with *Kpn*I and *Sap*I and transformed into CU428 cells by biolistic transformation. The ORF interval deleted for each of the targeted genes was as follows: *CTH1*, –34–925; *CTH2*, 1–922; *CTH3*, –23–991, and; *CAR1*, –86–858.

Biolistic transformation

Biolistic transformations were as described previously (Chilcoat *et al.*, 1996), with the following modifications: gold particles (Seashell Technology, San Diego, CA) were prepared as recommended with 15 µg of total linearized plasmid DNA. To select for positive transformants, drug was added 4 h after bombardment to cultures swirled at 30°C. Transformants were selected in paromomycin sulfate (PMS, 120 µg/ml) and $CdCl_2$ (1 µg/ml). PMS-resistant transformants were identified after 3 d. Transformants were then serially transferred daily in increasing amounts of PMS for at least 4 wk before further testing. The concentration of PMS was increased to 15 mg/ml, and $CdCl_2$ was maintained at 0.5 µg/ml for *CTH1* knockout, whereas PMS was increased up to 6 mg/ml and $CdCl_2$ was maintained at 0.3 µg/ml for *CTH2*, *CTH3*, and *CAR1* knockouts. When cell growth began to slow at the most stringent conditions, the cultures were returned to 10 mg/ml PMS and 0.5 $CdCl_2$ (for *CTH1* knockout) and 4 mg/ml PMS and 0.4 $CdCl_2$ (for *CTH2*, *CTH3*, and *CAR1* knockouts).

RT-PCR assessment of CTH1-3 and CAR1 disruption

Total RNA was isolated as per manufacturer's instructions using the RNeasy Mini Kit (Qiagen, Valencia, CA). The forward and reverse primers used for *CTH1-3* and *CAR1* are given in Supplemental Table S2. The presence of the *CTH1-3* and *CAR1* transcripts was assayed by one-step RT-PCR (Qiagen) using primers (Supplemental Table S2) to amplify 400–500 base pairs of each gene. Gene knockouts were confirmed by the continued absence of the corresponding transcripts after 3 wk of growth in the absence of drug selection (four or five serial transfers/week). To confirm that equal amounts of cDNA were being amplified, control RT-PCR with primers specific for sortilin 3 (*SOR3*) were run in parallel. The specific band intensities were measured using ImageJ software (National Institutes of Health, Bethesda, MD).

Expression of Cth3p-GFP at endogenous locus

The pmEGFP-neo4 vector was previously described (Briguglio *et al.*, 2013). Monomeric EGFP (mEGFP) was fused to the C-terminus of *CTH3* (TTHERM_00321680) at the endogenous macronuclear locus via homologous recombination, using linearized pCTH3-mEGFP-neo4. This construct consists of the cDNA-derived ORF of *CTH3* (minus the stop codon) followed by mEGFP, the *BTU1* terminator, a neo4 drug resistance cassette, and ~800 base pairs of *CTH3* downstream genomic sequence. To create pCTH3-mEGFP-neo4, the cDNA of *CTH3* (lacking the stop codon) and ~800 base pairs of *CTH3* downstream genomic sequence were amplified and cloned into the *Bam*HI and *Hin*dIII sites of the pmEGFP-neo4, respectively, by In-Fusion cloning.

The pCTH3-mEGFP-neo4 vector was used as substrate to generate (^{139}Asp → Asn, ^{324}Asp → Asn) mutations, in which select GAC codons in *CTH3* were replaced by AAT using GeneArt Site-Directed Mutagenesis PLUS Kit (Invitrogen). All final constructs were confirmed by DNA sequencing. Constructs were linearized with *Xho*1 and *Nhe*1 and transformed into CU428.1 cells by biolistic transformation as described earlier. Initial transformants were selected based on paromomycin resistance and then serially transferred for 3–4 wk in increasing drug concentrations to drive fixation of the variant allele. Consistent with the complete or near-complete replacement of the endogenous locus by the variant, transformants maintained both Cth3p-GFP expression and drug resistance for at least 6 mo after initial selection.

Live-cell microscopy

For imaging cells expressing CFP-tagged fusion proteins, transformants were grown overnight in SPP media and then transferred to S medium (0.2% yeast extract, 0.003% iron EDTA, which reduces autofluorescence in food vacuoles) containing 1 µg/ml $CdCl_2$ for 16 h at 30°C, followed by 4 h in 10 mM Tris, pH 7.4, with 0.2 µg/ml $CdCl_2$ at 22°C. Cth3p-GFP cultures were analyzed after growing to density of 6×10^5 cells/ml unless otherwise indicated. Cells were then transferred to S medium at room temperature for 2–4 h. To localize simultaneously Cth3-GFP and LysoTracker (Invitrogen), cells were incubated for 5 min with 200 nM LysoTracker, and images were captured within 30 min thereafter. To localize simultaneously Cth3-GFP and FM4-64 (Life Technologies, Carlsbad, CA), cells were incubated for 5 min with 5 µM FM4-64 and then pelleted and resuspended in S medium, after which the cells were imaged at a range of time points.

Live *Tetrahymena* expressing CFP and GFP fusions were immobilized using 6% polyethylene oxide (PEO; molecular weight, ~900,000) and imaged at 22°C on a Leica SP5 II STED-CW Superresolution Laser Scanning Confocal Microscope (Leica, Wetzlar, Germany) or Marianas Yokogawa-type spinning-disk inverted confocal microscope (Intelligent Imaging Innovations, Denver, CO), respectively. Background signal was subtracted from images, which were then saved as JPEGs that were colored, denoised, and adjusted in brightness/contrast/gamma with the program Fiji (http://fiji.sc/Fiji).

Immunofluorescence

Cells were fixed and immunolabeled as described previously (Bowman and Turkewitz, 2001). Grl3p and Grt1p were visualized

using monoclonal antibodies 5E9 (1:9; Bowman *et al.*, 2005a) and 4D11 (1:5; Turkewitz and Kelly, 1992), respectively, followed by Texas red–conjugated goat anti-mouse antibody (1:100; Life Technologies). CFP- and GFP-tagged fusion proteins were visualized using rabbit anti-GFP (1:400; Invitrogen), respectively, followed by Alexa 488–conjugated anti-rabbit antibody (1:250). For simultaneous localization of proteases and mucocyst core proteins, cells were doubly immunolabeled with mouse mAb 5E9 and rabbit anti-GFP. Cells were imaged on a Leica SP5 II confocal microscope, and image data were analyzed as described earlier. Image stack movies showing colocalization are found in Supplemental Movies S1–S3.

Dibucaine stimulation assay

Dibucaine stimulation of exocytosis was as described previously (Rahaman *et al.*, 2009).

SDS–PAGE and Western blotting

To prepare whole-cell lysates, ~3×10^5 cells were pelleted, washed twice with 10 mM Tris, pH 7.4, and precipitated with 10% trichloroacetic acid (TCA). Precipitates were incubated on ice for 30 min, centrifuged (18,000 × *g*, 10 min, 4°C), washed with ice-cold acetone, repelleted (18,000 × *g*, 5 min, 4°C), and then dissolved in 2.5× SDS–PAGE sample buffer. We resolved 2×10^4 cell equivalents/lane by SDS–PAGE unless otherwise indicated. To starve the cells and collect secreted protein, cells were washed twice and then resuspended in 10 mM Tris (pH 7.4) for 4 h. Aliquots of 4 ml were underlaid with a pad of 400 µl of glycerol (2% wt/vol) and centrifuged at high speed in a clinical centrifuge, resulting in a cell pellet within the glycerol pad. A 1.7-ml amount of the supernatants was then carefully withdrawn and precipitated with TCA after the addition of 17 µl 2% deoxycholate (DOC).

GFP-tagged fusion proteins were immunoprecipitated from detergent lysates using polyclonal rabbit anti-GFP antiserum as described previously (Briguglio *et al.*, 2013). For Western blots, samples were resolved by SDS–PAGE and transferred to 0.45-µm polyvinylidene fluoride (PVDF) membranes (Thermo Scientific, Rockford, IL). Blots were blocked and probed as previously described (Turkewitz *et al.*, 1991). The rabbit anti-Grl1p, rabbit anti-Grl3p, rabbit anti-Grl4p, rabbit anti-Grl8p, rabbit anti-polyG (Xie *et al.*, 2007), and mouse monoclonal anti-GFP (Covance, Princeton, NJ) primary antibodies were diluted 1:2000, 1:800, 1:250, 1:3000, 1:10,000, and 1:5000 respectively. Protein was visualized with either enhanced chemiluminescence horseradish peroxidase–linked anti-rabbit (NA934) or anti-mouse (NA931; Amersham Biosciences, Little Chalfont, United Kingdom) secondary antibody diluted 1:20,000 and SuperSignal West Femto Maximum Sensitivity Substrate (Thermo Scientific).

In vitro enzyme assay for Cth3p activity

Cth3 activity was assayed in vitro using the SensoLyte 520 Cathepsin D Assay Kit Fluorimetric (AnaSpec, Fremont, CA) as per manufacturer's instruction and including the cathepsin D positive control provided by the manufacturer. Cth3p, in parallel with the active-site mutant, was isolated as GFP fusion (cth3-4p and cth3-5-p, respectively) by immunoprecipitation from *Tetrahymena* whole-cell detergent lysate using polyclonal rabbit anti-GFP antiserum as described, except that the following protease inhibitors were included in the lysis buffer: 10 µM E-64, 1 mM phenylmethylsulfonyl fluoride, and 100 µM leupeptin. Enzyme assays were carried out in 100 µl in 96-well plates. Activity was recorded as the rate of hydrolysis of substrate at 5- min intervals for 60 min at room temperature, using a Gemini XPS Fluorescence Microplate Reader (excitation, 485 nm; emission, 515 nm; Molecular Devices, Sunnyvale, CA).

Gene expression profiles

Expression profiles were derived from the *Tetrahymena* Functional Genomics Database (http://tfgd.ihb.ac.cn/).

Phylogenetic tree construction

Using protein BLAST (blastp), the *T. thermophila CTH1*, *CTH2*, and *CTH3* genes were used to identify potential homologues in ciliates, apicomplexans, *Arabidopsis*, and *H. sapiens*, listed in Supplemental Table S3. Similarly, the *T. thermophila CAR1* sequence was used to identify homologues in ciliates, listed in Supplemental Table S4. For tree building, the top hits were selected from each lineage, assembled, and aligned with ClustalX (1.8), and maximum-likelihood trees were constructed with MEGA5 (Molecular Evolutionary Genetics Analysis: www.megasoftware.net/). Gapped regions were excluded in a complete manner, and percentage bootstrap values from 1000 replicates were derived.

In silico analyses

The coding sequence of the aspartic proteases, cysteine proteases, and zinc carboxypeptidase were analyzed for conserved active site residues by the National Center for Biotechnology Information Conserved Domain Database and protein BLAST (Marchler-Bauer *et al.*, 2009) and for signal peptides by SignalP (Emanuelsson *et al.*, 2007). Alignment of protein sequences was performed using ClustalX (1.8) with default parameters.

ACKNOWLEDGMENTS

We are grateful to Cassie Kontur and Mahima Joiya for support, Vytas Bindokas and Christine Labno (University of Chicago Light Microscopy Core Facility) for help with light microscopy, and Vernon Carruthers (University of Michigan, Ann Arbor, MI), Eileen Hamilton (University of Californina, Santa Barbara, Santa Barbara, CA), and Lydia Bright (Indiana University, Bloomington, IN) for advice. Doug Chalker (Washington University, St. Louis, MO) generously shared *Tetrahymena*-specific tagging vectors, Jody Bowen (University of Rochester, Rochester, NY) and Jacek Gaertig (University of Georgia, Athens, GA) shared anti-tubulin antibodies, and E. Marlo Nelsen and Joseph Frankel (University of Iowa, Iowa City, IA) shared mAbs 4D11 and 5E9. This research was supported by National Science Foundation MCB-1051985 to A.P.T. A.P.T. serves on the scientific advisory board of Tetragenetics (Cambridge, MA).

REFERENCES

Adoutte A (1988). Exocytosis: biogenesis, transport and secretion of trichocysts. In: Paramecium, Berlin: Springer-Verlag, 325–362.

Adoutte A, Garreau de Loubresse N, Beisson J (1984). Proteolytic cleavage and maturation of the crystalline secretion products of *Paramecium*. J Mol Biol 180, 1065–1081.

Ahras M, Otto GP, Tooze SA (2006). Synaptotagmin IV is necessary for the maturation of secretory granules in PC12 cells. J Cell Biol 173, 241–251.

Allen RD (1967). Fine structure, reconstruction and possible functions of components of the cortex of *Tetrahymena pyriformis*. J Protozool 14, 553–565.

Arvan P, Castle D (1998). Sorting and storage during secretory granule biogenesis: looking backward and looking forward. Biochem J 332, 593–610.

Bendayan M (1989). Ultrastructural localization of insulin and C-peptide antigenic sites in rat pancreatic B cell obtained by applying the quantitative high-resolution protein A-gold approach. Am J Anat 185, 205–216.

Bonnemaison ML, Eipper BA, Mains RE (2013). Role of adaptor proteins in secretory granule biogenesis and maturation. Front Endocrinol 4, 101.
Bowman GR, Elde NC, Morgan G, Winey M, Turkewitz AP (2005a). Core formation and the acquisition of fusion competence are linked during secretory granule maturation in *Tetrahymena*. Traffic 6, 303–323.
Bowman GR, Smith DG, Michael Siu KW, Pearlman RE, Turkewitz AP (2005b). Genomic and proteomic evidence for a second family of dense core granule cargo proteins in *Tetrahymena thermophila*. J Eukaryot Microbiol 52, 291–297.
Bowman GR, Turkewitz AP (2001). Analysis of a mutant exhibiting conditional sorting to dense core secretory granules in *Tetrahymena thermophila*. Genetics 159, 1605–1616.
Bradshaw NR, Chilcoat ND, Verbsky JW, Turkewitz AP (2003). Proprotein processing within secretory dense core granules of *Tetrahymena thermophila*. J Biol Chem 278, 4087–4095.
Bright LJ, Kambesis N, Nelson SB, Jeong B, Turkewitz AP (2010). Comprehensive analysis reveals dynamic and evolutionary plasticity of Rab GTPases and membrane traffic in *Tetrahymena thermophila*. PLoS Genet 6, e1001155.
Briguglio JS, Kumar S, Turkewitz AP (2013). Lysosomal sorting receptors are essential for secretory granule biogenesis in *Tetrahymena*. J Cell Biol 203, 537–550.
Cassidy-Hanley D, Bowen J, Lee JH, Cole E, VerPlank LA, Gaertig J, Gorovsky MA, Bruns PJ (1997). Germline and somatic transformation of mating *Tetrahymena thermophila* by particle bombardment. Genetics 146, 135–147.
Chanat E, Huttner WB (1991). Milieu-induced, selective aggregation of regulated secretory proteins in the *trans*-Golgi network. J Cell Biol 115, 1505–1519.
Chilcoat ND, Melia SM, Haddad A, Turkewitz AP (1996). Granule lattice protein 1 (Grl1p), an acidic, calcium-binding protein in *Tetrahymena thermophila* dense-core secretory granules, influences granule size, shape, content organization, and release but not protein sorting or condensation. J Cell Biol 135, 1775–1787.
Collins T, Wilhelm JM (1981). Post-translational cleavage of mucocyst precursors in *Tetrahymena*. J Biol Chem 256, 10475–10484.
Cowan AT, Bowman GR, Edwards KF, Emerson JJ, Turkewitz AP (2005). Genetic, genomic, and functional analysis of the granule lattice proteins in *Tetrahymena* secretory granules. Mol Biol Cell 16, 4046–4060.
Coyne RS *et al*. (2008). Refined annotation and assembly of the *Tetrahymena thermophila* genome sequence through EST analysis, comparative genomic hybridization, and targeted gap closure. BMC Genomics 9, 562.
Creemers JW, Jackson RS, Hutton JC (1998). Molecular and cellular regulation of prohormone processing. Semin Cell Dev Biol 9, 3–10.
Crump CM, Xiang Y, Thomas L, Gu F, Austin C, Tooze SA, Thomas G (2001). PACS-1 binding to adaptors is required for acidic cluster motif-mediated protein traffic. EMBO J 20, 2191–2201.
Ding Y, Ron A, Satir BH (1991). A potential mucus precursor in *Tetrahymena* wild type and mutant cells. J Protozool 38, 613–623.
Dodson G, Steiner D (1998). The role of assembly in insulin's biosynthesis. Curr Opin Struct Biol 8, 189–194.
Dou Z, Carruthers VB (2011). Cathepsin proteases in *Toxoplasma gondii*. Adv Exp Med Biol 712, 49–61.
Dou Z, Coppens I, Carruthers VB (2013). Non-canonical maturation of two papain-family proteases in *Toxoplasma gondii*. J Biol Chem 288, 3523–3534.
Eisen JA *et al*. (2006). Macronuclear genome sequence of the ciliate *Tetrahymena thermophila*, a model eukaryote. PLoS Biol 4, e286.
Elde NC, Long M, Turkewitz AP (2007). A role for convergent evolution in the secretory life of cells. Trends Cell Biol 17, 157–164.
Elde NC, Morgan G, Winey M, Sperling L, Turkewitz AP (2005). Elucidation of clathrin-mediated endocytosis in *Tetrahymena* reveals an evolutionarily convergent recruitment of dynamin. PLoS Genet 1, e52.
Emanuelsson O, Brunak S, von Heijne G, Nielsen H (2007). Locating proteins in the cell using TargetP, SignalP and related tools. Nat Protoc 2, 953–971.
Gautier MC, Sperling L, Madeddu L (1996). Cloning and sequence analysis of genes coding for *Paramecium* secretory granule (trichocyst) proteins. J Biol Chem 271, 10247–10255.
Glondu M, Coopman P, Laurent-Matha V, Garcia M, Rochefort H, Liaudet-Coopman E (2001). A mutated cathepsin-D devoid of its catalytic activity stimulates the growth of cancer cells. Oncogene 20, 6920–6929.
Gurkan C, Lapp H, Alory C, Su AI, Hogenesch JB, Balch WE (2005). Large-scale profiling of Rab GTPase trafficking networks: the membrome. Mol Biol Cell 16, 3847–3864.
Gutierrez JC, Orias E (1992). Genetic characterization of *Tetrahymena thermophila* mutants unable to secrete capsules. Dev Genet 13, 160–166.
Haddad A, Bowman GR, Turkewitz AP (2002). A new class of cargo protein in *Tetrahymena thermophila* dense core secretory granules. Eukaryot Cell 1, 583–593.
Hook V *et al*. (2004). Cathepsin L and Arg/Lys aminopeptidase: a distinct prohormone processing pathway for the biosynthesis of peptide neurotransmitters and hormones. Biol Chem 385, 473–480.
Hook V, Funkelstein L, Lu D, Bark S, Wegrzyn J, Hwang SR (2008). Proteases for processing proneuropeptides into peptide neurotransmitters and hormones. Annu Rev Pharmacol Toxicol 48, 393–423.
Hunseler P, Tiedtke A (1992). Genetic characterization of the secretory mutant MS-1 of *Tetrahymena thermophila*: vacuolarization and block in secretion of lysosomal hydrolases are caused by a single gene mutation. Dev Genet 13, 167–173.
Jacobs ME, DeSouza LV, Samaranayake H, Pearlman RE, Siu KW, Klobutcher LA (2006). The *Tetrahymena thermophila* phagosome proteome. Eukaryot Cell 5, 1990–2000.
Karrer KM ((2000). *Tetrahymena* genetics: two nuclei are better than one. Methods Cell Biol 62, 127–186.
Kim T, Gondre-Lewis MC, Arnaoutova I, Loh YP (2006). Dense-core secretory granule biogenesis. Physiology (Bethesda) 21, 124–133.
Kiy T, Vosskuhler C, Rasmussen L, Tiedtke A (1993). Three pools of lysosomal enzymes in *Tetrahymena thermophila*. Exp Cell Res 205, 286–292.
Klumperman J, Kuliawat R, Griffith JM, Geuze HJ, Arvan P (1998). Mannose 6-phosphate receptors are sorted from immature secretory granules via adaptor protein AP-1, clathrin, and syntaxin 6-positive vesicles. J Cell Biol 141, 359–371.
Knoll G, Haacke-Bell B, Plattner H (1991). Local trichocyst exocytosis provides an efficient escape mechanism for *Paramecium* cells. Eur J Protistol 27, 381–385.
Krieger TJ, Hook VY (1992). Purification and characterization of a cathepsin D protease from bovine chromaffin granules. Biochemistry 31, 4223–4231.
Madeddu L, Gautier MC, Le Caer JP, Garreau de Loubresse N, Sperling L (1994). Protein processing and morphogenesis of secretory granules in Paramecium. Biochimie 76, 329–335.
Marchler-Bauer A *et al*. (2009). CDD: specific functional annotation with the Conserved Domain Database. Nucleic Acids Res 37, D205–D210.
McKerrow JH (1999). Development of cysteine protease inhibitors as chemotherapy for parasitic diseases: insights on safety, target validation, and mechanism of action. Int J Parasitol 29, 833–837.
Melia SM, Cole ES, Turkewitz AP (1998). Mutational analysis of regulated exocytosis in *Tetrahymena*. J Cell Sci 111, 131–140.
Miao W, Xiong J, Bowen J, Wang W, Liu Y, Braguinets O, Grigull J, Pearlman RE, Orias E, Gorovsky MA (2009). Microarray analyses of gene expression during the *Tetrahymena thermophila* life cycle. PLoS One 4, e4429.
Michael J, Carroll R, Swift HH, Steiner DF (1987). Studies on the molecular organization of rat insulin secretory granules. J Biol Chem 262, 16531–16535.
Molinete M, Irminger JC, Tooze SA, Halban PA (2000). Trafficking/sorting and granule biogenesis in the beta-cell. Semin Cell Dev Biol 11, 243–251.
Morvan J, Tooze SA (2008). Discovery and progress in our understanding of the regulated secretory pathway in neuroendocrine cells. Histochem Cell Biol 129, 243–252.
Nusblat AD, Bright LJ, Turkewitz AP (2012). Conservation and innovation in *Tetrahymena* membrane traffic: proteins, lipids, and compartments. Methods Cell Biol 109, 141–175.
Orci L, Ravazzola M, Amherdt M, Madsen O, Vassalli JD, Perrelet A (1985). Direct identification of prohormone conversion site in insulin-secreting cells. Cell 42, 671–681.
Orci L, Ravazzola M, Amherdt M, Perrelet A, Powell SK, Quinn DL, Moore HP (1987). The trans-most cisternae of the Golgi complex: a compartment for sorting of secretory and plasma membrane proteins. Cell 51, 1039–1051.
Orias E, Flacks M, Satir BH (1983). Isolation and ultrastructural characterization of secretory mutants of *Tetrahymena thermophila*. J Cell Sci 64, 49–67.
Que X, Engel JC, Ferguson D, Wunderlich A, Tomavo S, Reed SL (2007). Cathepsin Cs are key for the intracellular survival of the protozoan parasite, *Toxoplasma gondii*. J Biol Chem 282, 4994–5003.
Que X, Ngo H, Lawton J, Gray M, Liu Q, Engel J, Brinen L, Ghosh P, Joiner KA, Reed SL (2002). The cathepsin B of *Toxoplasma gondii*, toxopain-1,

is critical for parasite invasion and rhoptry protein processing. J Biol Chem 277, 25791–25797.
Rahaman A, Miao W, Turkewitz AP (2009). Independent transport and sorting of functionally distinct protein families in *Tetrahymena* dense core secretory granules. Eukaryot Cell 8, 1575–1583.
Satir B (1977). Dibucaine-induced synchronous mucocyst secretion in *Tetrahymena*. Cell Biol Int Rep 1, 69–73.
Shang Y, Song X, Bowen J, Corstanje R, Gao Y, Gaertig J, Gorovsky MA (2002). A robust inducible-repressible promoter greatly facilitates gene knockouts, conditional expression, and overexpression of homologous and heterologous genes in *Tetrahymena thermophila*. Proc Natl Acad Sci USA 99, 3734–3739.
Shea M, Jakle U, Liu Q, Berry C, Joiner KA, Soldati-Favre D (2007). A family of aspartic proteases and a novel, dynamic and cell-cycle-dependent protease localization in the secretory pathway of *Toxoplasma gondii*. Traffic 8, 1018–1034.
Steiner DF (1991). Prohormone convertases revealed at last. Curr Biol 1, 375–377.
Steiner DF (1998). The proprotein convertases. Curr Opin Chem Biol 2, 31–39.
Stover NA, Rice JD (2011). Distinct cyclin genes define each stage of ciliate conjugation. Cell Cycle 10, 1699–1701.
Tiedtke A (1976). Capsule shedding in *Tetrahymena*. Naturwissenschaften 63, 93.
Tooze SA, Martens GJ, Huttner WB (2001). Secretory granule biogenesis: rafting to the SNARE. Trends Cell Biol 11, 116–122.
Turkewitz AP (2004). Out with a bang! *Tetrahymena* as a model system to study secretory granule biogenesis. Traffic 5, 63–68.
Turkewitz AP, Kelly RB (1992). Immunocytochemical analysis of secretion mutants of *Tetrahymena* using a mucocyst-specific monoclonal antibody. Dev Genet 13, 151–159.
Turkewitz AP, Madeddu L, Kelly RB (1991). Maturation of dense core granules in wild type and mutant *Tetrahymena thermophila*. EMBO J 10, 1979–1987.
Tyynela J, Sohar I, Sleat DE, Gin RM, Donnelly RJ, Baumann M, Haltia M, Lobel P (2000). A mutation in the ovine cathepsin D gene causes a congenital lysosomal storage disease with profound neurodegeneration. EMBO J 19, 2786–2792.
Vayssie L, Garreau De Loubresse N, Sperling L (2001). Growth and form of secretory granules involves stepwise assembly but not differential sorting of a family of secretory proteins in *Paramecium*. J Cell Sci 114, 875–886.
Vayssie L, Skouri F, Sperling L, Cohen J (2000). Molecular genetics of regulated secretion in *Paramecium*. Biochimie 82, 269–288.
Verbsky JW, Turkewitz AP (1998). Proteolytic processing and Ca2+-binding activity of dense-core vesicle polypeptides in *Tetrahymena*. Mol Biol Cell 9, 497–511.
Xie R, Clark KM, Gorovsky MA (2007). Endoplasmic reticulum retention signal-dependent glycylation of the Hsp70/Grp170-related Pgp1p in *Tetrahymena*. Eukaryotic Cell 6, 388–397.
Xiong J, Lu Y, Feng J, Yuan D, Tian M, Chang Y, Fu C, Wang G, Zeng H, Miao W (2013). *Tetrahymena* functional genomics database (TetraFGD): an integrated resource for *Tetrahymena* functional genomics. Database (Oxford) 2013, bat008.
Xiong J, Yuan D, Fillingham JS, Garg J, Lu X, Chang Y, Liu Y, Fu C, Pearlman RE, Miao W (2011). Gene network landscape of the ciliate *Tetrahymena thermophila*. PLoS One 6, e20124.
Xu J, Tian H, Wang W, Liang A (2012). The zinc finger protein Zfr1p is localized specifically to conjugation junction and required for sexual development in *Tetrahymena thermophila*. PLoS One 7, e52799.
Yao MC, Yao CH, Halasz LM, Fuller P, Rexer CH, Wang SH, Jain R, Coyne RS, Chalker DL (2007). Identification of novel chromatin-associated proteins involved in programmed genome rearrangements in *Tetrahymena*. J Cell Sci 120, 1978–1989.
Zaidi N, Maurer A, Nieke S, Kalbacher H (2008). Cathepsin D: a cellular roadmap. Biochem Biophys Res Commun 376, 5–9.
Zufall RA, McGrath CL, Muse SV, Katz LA (2006). Genome architecture drives protein evolution in ciliates. Mol Biol Evol 23, 1681–1687.